Available online at www.sciencedirect.com
SCIENCE DIRECT®
Comput. Methods Appl. Mech. Engrg. 193 (2004) 2357–2381
Computer methods in applied mechanics and engineering
www.elsevier.com/locate/cma

Material forces in open system mechanics

Ellen Kuhl, Paul Steinmann *

Department of Mechanical Engineering, Chair for Applied Mechanics, University of Kaiserslautern, Postfach 3049, D-67653 Kaiserslautern, Germany

Received 23 August 2002; received in revised form 7 November 2003; accepted 5 January 2004

Abstract

The basic concern of the present work is the exploitation of the notion of material forces in the theoretical and computational analysis of open systems with particular application to biomechanical problems. Based on a completely dual framework for the spatial and the material motion problem, we introduce the balance equations for open system thermodynamics. In combination with the appropriate constitutive equations, they constitute the basis of the finite element formulation derived thereafter. For the spatial motion problem, the solution of the governing equations, basically the balance of mass and momentum, renders the discrete nodal values of the density and the deformation as primary unknowns. For the material motion problem, the computational analysis of the balance of momentum yields the discrete material node point forces which can be interpreted as driving forces for the local rearrangement of material inhomogeneities. Once the spatial motion problem has been solved, the material force method is nothing but a mere post-processing step from an algorithmic point of view. As a convincing benefit of the proposed strategy, the computation of the material forces is extremely cheap and requires no additional finite element data structure. In the context of biomechanics, material forces give further insight into complex biomechanically induced processes, such as functional adaption, morphogenesis, healing or growth. For example, material forces on the boundary can be considered as a measure of shape sensitivity and thus indicate morphological changes while material forces in the interior indicate the tendency to create new mass locally or to equilibrate local density inhomogeneities.

Keywords: Spatial and material setting; Material inhomogeneities; Material force method; Open system mechanics; Biomechanics

1. Introduction

The theoretical and numerical analysis of open systems has experienced a remarkably growing interest within the last decade. This tendency is primarily driven by the interdisciplinary research in experimental and theoretical bio- and chemomechanics supplemented by recent computational developments. Unlike classical closed systems, open systems are allowed to exchange mass, momentum, energy and entropy with their environment. Consequently, the traditional balance equations for closed systems have to be enhanced

* Corresponding author. Tel.: +49-631-205-2419; fax: +49-631-205-2128.
E-mail addresses: ekuhl@rhrk.uni-kl.de (E. Kuhl), ps@rhrk.uni-kl.de (P. Steinmann).
URL: http://mechanik.mv.uni-kl.de.

0045-7825/$ - see front matter
doi:10.1016/j.cma.2004.01.022

by additional source terms that take into account the interaction with the outside world, see Cowin and Hegedus [6]. In recent theories, the influence of the environment has not a priori been restricted to source terms by additionally allowing for a possible in- or outflow of matter, see Epstein and Maugin [9] or Kuhl and Steinmann [24]. However, the definition of an appropriate constitutive equation for the mass flux is still an open issue. It should be mentioned that alternatively to open system mechanics, another prominent approach has been presented recently by Rodriguez et al. [38] who describe growth of soft tissues in terms of a growth tensor defining an incompatible reference configuration, compare also Garikipati et al. [13] for a slightly modified approach.

Nevertheless, we shall focus on the open system approach in the sequel. The number of phenomena that require an open system characterization is enormous. Typical examples taken from biomechanics are growth in soft and hard tissues, morphogenesis, self-healing phenomena in medical problems or the functional adaption of biological microstructures, just to mention a few. For a detailed description of the above mentioned processes the reader is referred to the outstanding monograph by Taber [44] or the recent textbooks by Carter and Beaupré [4] or Humphrey [20]. All these phenomena are primarily characterized through the fact, that the local amount of mass continuously adapts to the current environmental situation, particularly to changes in mechanical loading. This process of adaption is typically accompanied by the local reorganization of material inhomogeneities which can be described most elegantly within the material setting.

The material motion approach which represents an active branch of current research was originally introduced by Eshelby [10,11] who was the first to introduce material forces as forces acting on defects. Unlike physical forces, material forces act on the material manifold and represent the tendency of various types of inhomogeneities to move relative to the ambient material. Different alternative strategies towards a material motion framework have been suggested in the literature upon which we shall only mention the recent textbooks by Maugin [32], Gurtin [17], Kienzler and Herrmann [23] and Silhavý [40] and the excellent monographs by Maugin [33], Gurtin [16] and Epstein and Maugin [8,9] and references therein. Herein, the derivation of the material motion problem will be guided by arguments of duality as suggested by Shield [39] and specified recently by Steinmann [41,42] for closed system thermodynamics and by Kuhl and Steinmann [25] for the thermodynamics of open systems. Since material forces essentially indicate the local reorganization of material inhomogeneities, they are predestinated for biomechanical applications. They can be understood as driving forces for growth and healing processes, they motivate the introduction of a mass flux and suggest a possible constitutive equation for mass diffusion. Moreover, they can be interpreted as indicators for remodeling and morphogenesis.

For the spatial motion problem, first attempts towards a numerical simulation of biomechanical problems with the help of the finite element method date back to the early 1990s. Nevertheless, these first computational simulations were basically restricted to hard tissue mechanics for which a geometrically linear approach yielded sufficiently accurate results, see e.g. Beaupré et al. [2], Jacobs et al. [21,22], Weinans et al. [45,46], Harrigan and Hamilton [18,19], Pettermann et al. [36] and Reiter [37] or Kuhl et al. [27] for an extended comparison of the different approaches. Typically, next to the momentum balance which characterizes the mechanical equilibrium, the balance of mass is taken into account as biological equilibrium equation. The solution of the resulting set of non-linear equations yields the discrete node point values of the density and the deformation which furnish the primary unknowns.

The numerical evaluation of the material motion problem with the help of the finite element method represents an area of active research. Herein, we shall make use of the material force method as advocated by Steinmann et al. [43] and Denzer et al. [7] in the context of linear and non-linear elastic fracture mechanics. Thereby, the momentum balance of the material motion problem is cast into its weak form and discretized in space with the classical Galerkin based finite element technique. Once the solution of the spatial motion problem has been determined, the evaluation of the discrete material node point forces is straightforward since it requires no additional finite element data structures or expensive inversions of system matrices. Due to its computational simplicity, the material force method has been applied to various

different physical phenomena recently, such as damage mechanics by Liebe et al. [31], tire mechanics by Govindjee [15], thermomechanics by Kuhl et al. [29] or classical fracture mechanics by Müller et al. [34] and Müller and Maugin [35]. Discrete material forces typically point in the direction of a potential energy increase upon replacement of the material node point positions, thus indicating the growth of a crack in the opposite direction. Spurious material forces indicate that changes in node point positions of the finite element discretization yield an improved mesh with less potential energy. Braun [3] and Kuhl et al. [1,30] have made use of this property recently by applying material forces as indicators for the quality of the finite element mesh. The application of the material force method is far-reaching and not yet fully explored. Nevertheless, we believe that the method is particularly suited for biomechanical applications since living materials show the remarkable ability to continuously interact with their environment and adapt to environmental changes. Material forces are believed to give additional insight into the understanding of mechanical factors that drive biological processes as healing or growth. Their knowledge thus enables a natural assessment of complex biomechanical phenomena such as functional adaption or morphogenesis. To illustrate the first attempts towards utilizing the material force method in open system mechanics is the fundamental aim of this contribution.

The paper is organized as follows. After briefly summarizing the geometrically non-linear kinematics of the spatial and the material setting in Section 2, we shall introduce the balance equations for open system thermodynamics in Section 3. The choice of appropriate constitutive equations is the subject of Section 4. Guided by concepts of duality, we then discuss the spatial and material force balance in strong and weak form in Section 5. The latter naturally lends itself to the Galerkin type finite element discretization derived in Section 6. Finally, the suggested algorithm is evaluated with the help of selected examples of mass diffusion, functional adaption and healing in Section 7. The contribution ends with final conclusions and an outlook on future perspectives in Section 8.

2. Kinematics

To introduce our notation, we shall briefly review the underlying geometrically non-linear kinematics of the spatial and the material motion problem. Thereby, the classical spatial motion problem, which is sometimes introduced as "direct motion problem" is based on the idea of following "physical particles" from a fixed material position $\boldsymbol{X}$ through the ambient space. In contrast to this, within the material motion or "inverse motion problem", "physical particles" are followed through the ambient material at fixed spatial position $\boldsymbol{x}$.

2.1. Spatial motion problem

The spatial motion problem is characterized through the spatial deformation map

$$\boldsymbol{x} = \boldsymbol{\varphi}(\boldsymbol{X}, t): \quad \mathscr{B}_0 \to \mathscr{B}_t \tag{1}$$

mapping the material placement $\boldsymbol{X}$ of a "physical particle" in the material configuration $\mathscr{B}_0$ to the spatial placement $\boldsymbol{x}$ of the same "physical particle" in the spatial configuration $\mathscr{B}_t$, see Fig. 1. The related spatial deformation gradient $\boldsymbol{F}$ and its Jacobian J

$$\boldsymbol{F} = \nabla_X \boldsymbol{\varphi}(\boldsymbol{X}, t): \quad T\mathscr{B}_0 \to T\mathscr{B}_t \quad J = \det \boldsymbol{F} > 0 \tag{2}$$

define the linear tangent map from the fixed material tangent space $T\mathscr{B}_0$ to the time-dependent tangent space $T\mathscr{B}_t$. Moreover, with the material time derivative D_t of an arbitrary quantity $\{\bullet\}$ at fixed material placement $\boldsymbol{X}$ as $\mathrm{D}_t\{\bullet\} = \partial_t\{\bullet\}|_X$, the spatial velocity $\boldsymbol{v} = \mathrm{D}_t\boldsymbol{\varphi}(\boldsymbol{X}, t)$ can be introduced as the material time derivative of the spatial deformation map $\boldsymbol{\varphi}$. Recall that its material gradient is equal to the material time

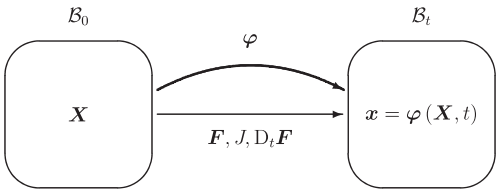

Fig. 1. Spatial motion problem: kinematics.

derivative of the spatial deformation gradient $\boldsymbol{F}$ as $\mathrm{D}_t\boldsymbol{F} = \nabla_X \boldsymbol{v}$. With the above definitions in hand, the material time derivative of the spatial motion Jacobian J can be expressed through the well-known Euler identity $\mathrm{D}_t J = J \operatorname{div} \boldsymbol{v}$ with $\operatorname{div} \boldsymbol{v} = \boldsymbol{F}^{-t} : \mathrm{D}_t\boldsymbol{F}$ denoting the spatial divergence of the spatial velocity $\boldsymbol{v}$. Note that in the following considerations, we shall assign the subscript D to any flux term referring to the material time derivative D_t of the related balanced quantity.

2.2. Material motion problem

In complete duality, we can introduce the material deformation map $\boldsymbol{\Phi}$ with

$$\boldsymbol{X} = \boldsymbol{\Phi}(\boldsymbol{x}, t): \quad \mathscr{B}_t \to \mathscr{B}_0 \tag{3}$$

defining the mapping of the spatial placement of a "physical particle" $\boldsymbol{x}$ in the spatial configuration $\mathscr{B}_t$ to the material placement of the same "physical particle" in the material configuration $\mathscr{B}_0$, see Fig. 2. The related linear tangent map from the fixed spatial tangent space $T\mathscr{B}_t$ to the material tangent space $T\mathscr{B}_0$ is defined through the material deformation gradient $\boldsymbol{f}$ and its Jacobian j:

$$\boldsymbol{f} = \nabla_x \boldsymbol{\Phi}(\boldsymbol{x}, t): \quad T\mathscr{B}_t \to T\mathscr{B}_0 \quad j = \det \boldsymbol{f} > 0. \tag{4}$$

With the definition of the spatial time derivative d_t of a quantity $\{\bullet\}$ at fixed spatial placements $\boldsymbol{x}$ as $\mathrm{d}_t\{\bullet\} = \partial_t\{\bullet\}|_x$ the material velocity $\boldsymbol{V} = \mathrm{d}_t\boldsymbol{\Phi}(\boldsymbol{x}, t)$ can be introduced as the spatial time derivative of the material motion map $\boldsymbol{\Phi}$. Its spatial gradient is equal to the spatial time derivative of the material motion deformation gradient $\boldsymbol{f}$ as $\mathrm{d}_t\boldsymbol{f} = \nabla_x \boldsymbol{V}$. Consequently, the spatial time derivative of the material motion Jacobian j can be expressed as $\mathrm{d}_t j = j \operatorname{div} \boldsymbol{V}$ whereby $\operatorname{div} \boldsymbol{V} = \boldsymbol{f}^{-t} : \mathrm{d}_t\boldsymbol{f}$ denotes the material divergence of the material velocity $\boldsymbol{V}$. In the dynamic context, we will use the subscript d with the flux terms of the balance equations to indicate their reference to the spatial time derivative d_t of the related balanced quantity.

Remark 2.1 (*Spatial vs. material motion kinematics*). The spatial and the material motion problem are related through the identity maps in $\mathscr{B}_0$ and $\mathscr{B}_t$. Consequently, the spatial and the material deformation gradient are simply related by their inverses $\boldsymbol{F}^{-1} = \boldsymbol{f}$ and $\boldsymbol{f}^{-1} = \boldsymbol{F}$. Moreover, we obtain the following fundamental relations between spatial and material velocities $\boldsymbol{V} = -\boldsymbol{f} \cdot \boldsymbol{v}$ and $\boldsymbol{v} = -\boldsymbol{F} \cdot \boldsymbol{V}$. The material and spatial time derivative D_t and d_t of any scalar- or vector-valued function $\{\bullet\}$ are related through the Euler

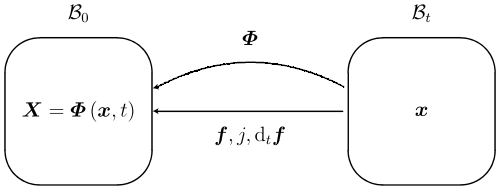

Fig. 2. Material motion problem: kinematics.

theorem in terms of the individual convective terms $\nabla_x\{\bullet\}\cdot\boldsymbol{v}$ and $\nabla_X\{\bullet\}\cdot\boldsymbol{V}$ as $\mathrm{D}_t\{\bullet\}=\mathrm{d}_t\{\bullet\}+\nabla_x\{\bullet\}\cdot\boldsymbol{v}$ and $\mathrm{d}_t\{\bullet\}=\mathrm{D}_t\{\bullet\}+\nabla_X\{\bullet\}\cdot\boldsymbol{V}$. Last, the material and spatial time derivative of a volume specific scalar- or vector-valued function $\{\bullet\}_0=\rho_0\{\bullet\}$ and $\{\bullet\}_t=\rho_t\{\bullet\}$ are related through the spatial and material motion version of Reynold's transport theorem as $j\,\mathrm{D}_t\{\bullet\}_0=\mathrm{d}_t\{\bullet\}_t+\operatorname{div}(\{\bullet\}_t\otimes\boldsymbol{v})$ and $J\,\mathrm{d}_t\{\bullet\}_t=\mathrm{D}_t\{\bullet\}_0+\operatorname{div}(\{\bullet\}_0\otimes\boldsymbol{V})$.

3. Balance equations

The present section briefly summarizes the balance equations for open system thermodynamics which constitute the basis for the finite element analysis to be derived later on. Unlike classical closed systems typically found in traditional mechanical applications, open systems exhibit a permanent exchange of mass, momentum, energy and entropy with their environment. As a natural consequence, the classical balance of mass has to be enhanced by an additional mass flux and a mass source. The impact of the open system on the higher balance equations is two-fold. On the one hand, an explicit exchange with the outside world can take place which manifests itself in the corresponding Neumann boundary conditions and the non-classical volume source terms. On the other hand, the newly added or in-flowing mass typically carries a certain amount of momentum, energy and entropy which has to be accounted for as well. The latter, however, is only visible in the so-called "volume specific" format of the balance equations, compare Kuhl and Steinmann [24,25]. Herein, we shall strictly stick to the "mass specific" format which is free from all the explicit mass dependent influences. Apart from the non-standard Neumann boundary conditions and the non-standard source term, it takes the familiar form known from classical closed system thermodynamics.

3.1. Spatial motion problem

We begin by introducing the balance equations for the spatial motion problem. The balance of mass

$$\mathrm{D}_t\rho_0=\operatorname{div}\boldsymbol{R}+\mathscr{R}_0+\mathsf{m}_0 \tag{5}$$

furnishes the fundamental relation in open system thermodynamics. It balances the rate of change of the reference density ρ_0 with a possible influx of mass $\boldsymbol{R}$ and a mass source $\mathscr{R}_0$. Note that for the sake of duality, we have introduced the additional convective term m_0, keeping in mind that this term vanishes identically for the spatial motion case as $\mathsf{m}_0=0$. The mass specific balance of momentum

$$\rho_0\mathrm{D}_t\boldsymbol{p}=\operatorname{div}\overline{\boldsymbol{\Pi}}^t_D+\overline{\boldsymbol{b}}_0-\mathsf{m}_0\boldsymbol{p} \tag{6}$$

balances the rate of change of the mass specific momentum density $\boldsymbol{p}=\boldsymbol{g}\cdot\boldsymbol{v}$ with the reduced momentum flux $\overline{\boldsymbol{\Pi}}^t_D$ and the reduced momentum source $\overline{\boldsymbol{b}}_0$. In the transient case, the dynamic momentum flux $\overline{\boldsymbol{\Pi}}^t_D$ is related to its static counterpart, the Piola–Kirchhoff stress tensor $\overline{\boldsymbol{\Pi}}^t$, via the kinetic energy K_0 as $\overline{\boldsymbol{\Pi}}^t_D=\overline{\boldsymbol{\Pi}}-\mathrm{D}_{\boldsymbol{F}}K_0=\overline{\boldsymbol{\Pi}}$. Moreover, we can introduce the mass specific balance of internal energy which can be derived as the difference of the total energy balance and the balance of kinetic energy, a weighted version of the above stated balance of momentum. As a consequence, the rate of change of the mass specific internal energy I is required to be in equilibrium with the reduced non-mechanical energy flux $\overline{\boldsymbol{Q}}_D$, the reduced non-mechanical energy source $\overline{\mathscr{Q}}_0$ and the internal power $\mathsf{p}_0^{\mathrm{int}}=\overline{\boldsymbol{\Pi}}^t:\mathrm{D}_t\boldsymbol{F}-\boldsymbol{v}\cdot\overline{\boldsymbol{b}}_0^{\mathrm{int}}$,

$$\rho_0\mathrm{D}_tI=-\operatorname{div}\overline{\boldsymbol{Q}}_D+\overline{\mathscr{Q}}_0-\mathsf{m}_0I+\mathsf{p}_0^{\mathrm{int}}, \tag{7}$$

whereby $\overline{\boldsymbol{b}}_0^{\mathrm{int}}=\boldsymbol{0}$ for the spatial motion case. Finally, the balance of entropy can be introduced as the rate of change of the mass specific entropy S being in equilibrium with the reduced entropy flux $\operatorname{div}\overline{\boldsymbol{H}}_D$, the reduced entropy source $\overline{\mathscr{H}}_0$ and the internal entropy production $\mathsf{h}_0^{\mathrm{int}}$ which is required to be non-negative throughout the entire thermodynamical process as $\mathsf{h}_0^{\mathrm{int}}\geqslant 0$:

$$\rho_0 \mathrm{D}_t S = -\mathrm{div}\,\overline{\boldsymbol{H}}_D + \overline{\mathscr{H}}_0 - \mathsf{m}_0 S + \mathsf{h}_0^{\mathrm{int}}. \tag{8}$$

By making use of the following relations between the reduced entropy flux $\overline{\boldsymbol{H}}_D$ and source $\overline{\mathscr{H}}_0$ and the reduced non-mechanical energy flux $\overline{\boldsymbol{Q}}_D$ and source $\overline{\mathscr{Q}}_0$ as $\overline{\boldsymbol{H}}_D = \overline{\boldsymbol{Q}}_D/\theta + \boldsymbol{S}$ and $\overline{\mathscr{H}}_0 = \overline{\mathscr{Q}}_0/\theta + \mathscr{S}_0$ we can derive the spatial motion version of the Clausius–Duhem inequality:

$$\overline{\mathsf{d}}_0 = \overline{\boldsymbol{\Pi}}^t : \mathrm{D}_t \boldsymbol{F} - \boldsymbol{v} \cdot \overline{\boldsymbol{b}}_0^{\mathrm{int}} - \rho_0 \mathrm{D}_t \Psi - \mathsf{m}_0 \Psi - \rho_0 S \mathrm{D}_t \theta + [\mathrm{div}\,\boldsymbol{S} - \mathscr{S}_0]\theta - \overline{\boldsymbol{Q}}_D \cdot \nabla_X \ln\theta \geqslant 0. \tag{9}$$

Herein, we have introduced the free energy Ψ through the classical Legendre–Fenchel transform as $\Psi = I - \theta S$. Moreover, we have included the non-standard extra terms $\boldsymbol{S}$ and $\mathscr{S}_0$ taking into account the explicit exchange of entropy with the outside world.

3.2. Material motion problem

At this stage, the balance equations of the material motion problem are formally introduced in complete analogy to their spatial motion counterparts guided by arguments of duality. Relations between the spatial and material motion quantities will be pointed out thereafter. Again, the balance of mass

$$\mathrm{d}_t \rho_t = \mathrm{div}\,\boldsymbol{r} + \mathscr{R}_t + \mathsf{M}_{\mathsf{t}} \tag{10}$$

represents the basic ingredient of open system thermodynamics. It balances the rate of change of the density ρ_t with the mass flux $\boldsymbol{r}$, the mass source $\mathscr{R}_t$ and a convective term $\mathsf{M}_{\mathsf{t}} = -\mathrm{div}(\rho_t \boldsymbol{v})$, which does not vanish for the material motion problem. The corresponding mass specific balance of momentum

$$\rho_t \mathrm{d}_t \boldsymbol{P} = \mathrm{div}\,\overline{\boldsymbol{\pi}}_d^t + \overline{\boldsymbol{B}}_t - \mathsf{M}_{\mathsf{t}} \boldsymbol{P} \tag{11}$$

states the equilibrium between the rate of change of the mass specific momentum density $\boldsymbol{P} = \boldsymbol{C} \cdot \boldsymbol{V}$, the reduced dynamic momentum flux $\overline{\boldsymbol{\pi}}_d^t$, the reduced momentum source $\overline{\boldsymbol{B}}_t$ and the convective term $\mathsf{M}_{\mathsf{t}} \boldsymbol{P}$. Again, the dynamic momentum flux $\overline{\boldsymbol{\pi}}_d^t$ can be related to the static momentum flux $\overline{\boldsymbol{\pi}}^t$ as $\overline{\boldsymbol{\pi}}_d^t = \overline{\boldsymbol{\pi}}^t - \mathrm{d}_f K_t$. Similar to the spatial motion problem, the balance of internal energy can be derived as the difference of the balance of total and kinetic energy. The rate of change of the mass specific internal energy I is thus required to be in equilibrium with the reduced non-mechanical energy flux $\overline{\boldsymbol{q}}_d$, the reduced non-mechanical energy source $\overline{\mathscr{Q}}_t$, the convective term $\mathsf{M}_{\mathsf{t}} I$ and the internal mechanical power $\mathsf{P}_{\mathsf{t}}^{\mathrm{int}} = \overline{\boldsymbol{\pi}}^t : \mathrm{d}_t \boldsymbol{f} - \boldsymbol{V} \cdot \overline{\boldsymbol{B}}_t^{\mathrm{int}}$:

$$\rho_t \mathrm{d}_t I = -\mathrm{div}\,\overline{\boldsymbol{q}}_d + \overline{\mathscr{Q}}_t - \mathsf{M}_{\mathsf{t}} I + \mathsf{P}_{\mathsf{t}}^{\mathrm{int}}. \tag{12}$$

Note however, that the reduced internal forces $\overline{\boldsymbol{B}}_t^{\mathrm{int}}$ do not vanish for the material motion case. Last, we can introduce the balance of entropy as the rate of change of the mass specific entropy S being in equilibrium with the reduced entropy flux $\mathrm{div}\,\overline{\boldsymbol{h}}_d$ and source $\overline{\mathscr{H}}_t$, the convective term $\mathsf{M}_{\mathsf{t}} S$ and the internal entropy production $\mathsf{H}_{\mathsf{t}}^{\mathrm{int}}$,

$$\rho_t \mathrm{d}_t S = -\mathrm{div}\,\overline{\boldsymbol{h}}_d + \overline{\mathscr{H}}_t - \mathsf{M}_{\mathsf{t}} S + \mathsf{H}_{\mathsf{t}}^{\mathrm{int}}, \tag{13}$$

whereby $\mathsf{H}_{\mathsf{t}}^{\mathrm{int}} \geqslant 0$. Accordingly, the material motion version of the Clausius–Duhem inequality follows by relating the reduced entropy flux $\overline{\boldsymbol{h}}_d$ and source $\overline{\mathscr{H}}_t$ to the reduced non-mechanical energy flux $\overline{\boldsymbol{q}}_d$ and source $\overline{\mathscr{Q}}_t$ in terms of the extra entropy flux and source $\boldsymbol{s}$ and $\mathscr{S}_t$ as $\overline{\boldsymbol{h}}_d = \overline{\boldsymbol{q}}_d/\theta + \boldsymbol{s}$ and $\overline{\mathscr{H}}_t = \overline{\mathscr{Q}}_t/\theta + \mathscr{S}_t$:

$$\overline{\mathsf{D}}_{\mathsf{t}} = \overline{\boldsymbol{\pi}}^t : \mathrm{d}_t \boldsymbol{f} - \overline{\boldsymbol{B}}_t^{\mathrm{int}} \cdot \boldsymbol{V} - \rho_t \mathrm{d}_t \Psi - \mathsf{M}_{\mathsf{t}} \Psi - \rho_t S \mathrm{d}_t \theta + [\mathrm{div}\,\boldsymbol{s} - \mathscr{S}_t]\theta - \overline{\boldsymbol{q}}_d \cdot \nabla_x \ln\theta \geqslant 0. \tag{14}$$

Remark 3.1 (*Spatial vs. material quantities*). The scalar-valued material motion balance of mass, internal energy and entropy basically follow from their spatial motion counterparts by a multiplication with the material motion Jacobian j. Consequently, we can set up the following relations between the material and spatial motion fluxes:

$$\boldsymbol{r} = j\boldsymbol{R}\cdot\boldsymbol{F}^t, \quad \boldsymbol{s} = j\boldsymbol{S}\cdot\boldsymbol{F}^t, \quad \overline{\boldsymbol{q}}_d = j\overline{\boldsymbol{Q}}_D\cdot\boldsymbol{F}^t + j\rho_0 S\theta\boldsymbol{v}, \quad \overline{\boldsymbol{h}}_d = j\overline{\boldsymbol{H}}_D\cdot\boldsymbol{F}^t + j\rho_0 S\boldsymbol{v}. \tag{15}$$

Therein, the first term on each righthand side arises from the corresponding Piola transforms while the terms $j\rho_0 S\theta\boldsymbol{v}$ and $j\rho_0 S\boldsymbol{v}$ represent the configurational non-mechanical energy increase and the configurational entropy increase, respectively, see e.g. Gurtin [17]. The corresponding source terms of the material and the spatial motion problem are simply related via the Jacobian j:

$$\mathscr{R}_t = j\mathscr{R}_0, \quad \mathscr{S}_t = j\mathscr{S}_0, \quad \overline{\mathscr{Q}}_t = j\overline{\mathscr{Q}}_0, \quad \overline{\mathscr{H}}_t = j\overline{\mathscr{H}}_0. \tag{16}$$

To set up relations between the material and the spatial motion momentum flux $\overline{\boldsymbol{\pi}}_d^t$ and $\overline{\boldsymbol{\Pi}}_D^t$ and the corresponding source terms $\overline{\boldsymbol{B}}_t$ and $\overline{\boldsymbol{b}}_0$ it is essential to further specify the constitutive equations. This will be shown in the following section.

Remark 3.2 (*Governing equations*). While the balance of entropy is classically satisfied a priori through the choice of appropriate constitutive equations, the balance of mass, momentum and internal energy constitute the set of field equations that govern the density, the deformation and the temperature field. Since biomechanical problems are typically considered as isothermal processes, the temperature no longer furnishes an independent variable. Consequently, we are left with the balance of mass and momentum which can be expressed as

$$\begin{aligned} \mathrm{D}_t\rho_0 &= \operatorname{div}\boldsymbol{R} + \mathscr{R}_0, \\ \rho_0\mathrm{D}_t\boldsymbol{p} &= \operatorname{div}\overline{\boldsymbol{\Pi}}_D^t + \overline{\boldsymbol{b}}_0, \end{aligned} \tag{17}$$

for the spatial motion case. Note that herein, the convective terms have been neglected, since $\mathsf{m}_0 = 0$. For the time discretization that will be performed later on, it becomes essential to replace the the spatial time derivatives $\mathrm{d}_t\rho_t$ and $\mathrm{d}_t\boldsymbol{P}$ of the balance of mass (10) and momentum (11) of the material motion problem by their material counterparts $j\mathrm{D}_t\rho_0$ and $\mathrm{D}_t\boldsymbol{P}$. However, this straightforward transformation is nothing but the application of Reynold's transport theorem as $\mathrm{d}_t\rho_t = j\mathrm{D}_t\rho_0 + \mathsf{M}_\mathrm{t}$ and of the Euler theorem as $\mathrm{d}_t\boldsymbol{P} = \mathrm{D}_t\boldsymbol{P} - \operatorname{div}(j\rho_0\boldsymbol{P}\otimes\boldsymbol{v}) - \mathsf{M}_\mathrm{t}\boldsymbol{P}$, compare Remark 2.1. Consequently, the additional convective M_t-terms of the material motion problem vanish identically and the dynamic momentum flux $\overline{\boldsymbol{\pi}}_d^t$ has to be replaced by $\overline{\boldsymbol{\pi}}_D^t = \overline{\boldsymbol{\pi}}_d^t + j\rho_0\boldsymbol{P}\otimes\boldsymbol{v}$. Accordingly, the material motion problem is primarily governed by the following set of equations:

$$\begin{aligned} j\,\mathrm{D}_t\rho_0 &= \operatorname{div}\boldsymbol{r} + \mathscr{R}_t, \\ \rho_t\mathrm{D}_t\boldsymbol{P} &= \operatorname{div}\overline{\boldsymbol{\pi}}_D^t + \overline{\boldsymbol{B}}_t. \end{aligned} \tag{18}$$

4. Constitutive equations

In what follows, we shall exploit the spatial and the material version of the Clausius–Duhem inequality defining fundamental restrictions for the choice of the constitutive response functions. The introduction of a potential for the reduced momentum flux finally enables us to formulate relations between the material and the spatial motion momentum fluxes and sources.

4.1. Spatial motion problem

For the spatial motion case, we shall assume the existence of a free energy function Ψ_0 which is multiplicatively decomposable into the reference density ρ_0 and the mass specific free energy Ψ as $\Psi_0 = \rho_0\Psi$.

Thereby, the latter is assumed to be a function of the reference density ρ_0 and the spatial motion deformation gradient $\boldsymbol{F}$ with a possible explicit dependence on the material placement $\boldsymbol{X}$ as $\Psi = \Psi(\rho_0, \boldsymbol{F}; \boldsymbol{X})$. Consequently, its material time derivative can be expanded as $\mathrm{D}_t\Psi = \mathrm{D}_{\rho_0}\Psi \mathrm{D}_t\rho_0 + \mathrm{D}_{\boldsymbol{F}}\Psi : \mathrm{D}_t\boldsymbol{F}$. The evaluation of the isothermal version of the Clausius–Duhem inequality (9), the so-called Clausius–Planck inequality,

$$\overline{\mathsf{d}}_0 = [\overline{\boldsymbol{\Pi}}^t - \rho_0 \mathrm{D}_{\boldsymbol{F}}\Psi] : \mathrm{D}_t\boldsymbol{F} - \overline{\boldsymbol{b}}_0^{\mathrm{int}} \cdot \boldsymbol{v} - \mathsf{m}_0\Psi - [\mathrm{div}\,\boldsymbol{R} - \mathscr{R}_0]\rho_0 \mathrm{D}_{\rho_0}\Psi + [\mathrm{div}\,\boldsymbol{S} - \mathscr{S}_0]\theta \geqslant 0, \tag{19}$$

with $\mathsf{m}_0 = 0$ defines the reduced momentum flux $\overline{\boldsymbol{\Pi}}^t$ as thermodynamically conjugate variable to the spatial motion deformation gradient $\boldsymbol{F}$. Moreover, we conclude that the spatial internal forces $\overline{\boldsymbol{b}}_0^{\mathrm{int}}$ have to vanish identically:

$$\overline{\boldsymbol{\Pi}}^t = \rho_0 \mathrm{D}_{\boldsymbol{F}}\Psi, \quad \overline{\boldsymbol{b}}_0^{\mathrm{int}} = \boldsymbol{0}. \tag{20}$$

Furthermore, we are left with the reduced dissipation inequality

$$\overline{\mathsf{d}}_0 = -[\mathrm{div}\,\boldsymbol{R} - \mathscr{R}_0]\rho_0 \mathrm{D}_{\rho_0}\Psi + [\mathrm{div}\,\boldsymbol{S} - \mathscr{S}_0]\theta \geqslant 0 \tag{21}$$

placing additional restrictions on the choice of the extra entropy flux and source $\boldsymbol{S}$ and $\mathscr{S}_0$ which at least have to compensate the dissipation generated by the mass flux and source $\boldsymbol{R}$ and $\mathscr{R}_0$. A typical specification of the free energy function for cellular materials like open-pored hard tissues is based on an elastic free energy, e.g. of Neo–Hooke type Ψ^{neo}, weighted by the actual relative density $[\rho_0/\rho_0^*]^n$, see Carter and Hayes [5] or Gibson and Ashby [14]:

$$\Psi = \left[\frac{\rho_0}{\rho_0^*}\right]^n \Psi^{\mathrm{neo}}, \quad \Psi^{\mathrm{neo}} = \frac{1}{\rho_0}\left[\frac{1}{2}\lambda \ln^2 J + \frac{1}{2}\mu[\boldsymbol{F} : \boldsymbol{F} - 3 - 2\ln J]\right]. \tag{22}$$

Herein, λ and μ denote the classical Lamé constants and n is a characteristic exponent varying between $1 \leqslant n \leqslant 3.5$ according to the degree of porosity of the material. The derivatives of the free energy Ψ with respect to the material density ρ_0 and the deformation gradient $\boldsymbol{F}$ take the following format,

$$\begin{aligned} \mathrm{D}_{\rho_0}\Psi &= [n-1]\left[\frac{\rho_0}{\rho_0^*}\right]^{[n-2]}\left[\frac{1}{\rho_0^*}\right]^2\left[\frac{1}{2}\lambda \ln^2 J + \frac{1}{2}\mu[\boldsymbol{F} : \boldsymbol{F} - 3 - 2\ln J]\right], \\ \mathrm{D}_{\boldsymbol{F}}\Psi &= \left[\frac{\rho_0}{\rho_0^*}\right]^{[n-1]}\left[\frac{1}{\rho_0^*}\right][\mu\boldsymbol{F} + [\lambda \ln J - \mu]\boldsymbol{F}^{-t}], \end{aligned} \tag{23}$$

whereby the first derivative can alternatively be expressed as $\mathrm{D}_{\rho_0}\Psi = [n-1]\Psi/\rho_0$. According to Eq. $(20)_1$, the reduced first Piola–Kirchhoff stress tensor

$$\overline{\boldsymbol{\Pi}}^t = \left[\frac{\rho_0}{\rho_0^*}\right]^n [\mu\boldsymbol{F} + [\lambda \ln J - \mu]\boldsymbol{F}^{-t}] \tag{24}$$

can be understood as the classical Neo–Hookean stress tensor weighted by the actual relative density $[\rho_0/\rho_0^*]^n$. For the sake of simplicity, the reduced momentum source $\overline{\boldsymbol{b}}_0$ is assumed to vanish identically:

$$\overline{\boldsymbol{b}}_0 = \boldsymbol{0}. \tag{25}$$

Paralleling the flux of concentrations introduced through Fick's law in chemomechanical applications, the mass flux $\boldsymbol{R}$ is related to the gradient of the density $\nabla_X\rho_0$ weighted by a mass conduction coefficient R_0. A related possible definition of the extra entropy flux $\boldsymbol{S}$ follows from the reduced dissipation inequality (21):

$$\boldsymbol{R} = R_0 \nabla_X \rho_0, \quad \boldsymbol{S} = [n-1]\Psi\frac{1}{\theta}R_0\nabla_X\rho_0. \tag{26}$$

In the context of hard tissue mechanics, we typically find variations of the following constitutive equation for the mass source $\mathscr{R}_0$,

$$\mathscr{R}_0 = \left[\frac{\rho_0}{\rho_0^*}\right]^{-m} \Psi_0 - \Psi_0^*, \quad \mathscr{S}_0 = -[n-1]\Psi\frac{1}{\theta}\left[\left[\frac{\rho_0}{\rho_0^*}\right]^{-m}\Psi_0 - \Psi_0^*\right], \tag{27}$$

whereby ρ_0^* and Ψ_0^* denote the reference density and the reference free energy, respectively, while m is an additional exponent. For stability reasons, the latter is commonly chosen to $m > n$, see Harrigan and Hamilton [19]. Again, a possible definition for the extra entropy source $\mathscr{S}_0$ follows from the dissipation inequality (21). In total, the model is thus defined through seven material parameters, the two Lamé constants λ and μ characterizing the elastic behavior of the basic material, the mass conduction coefficient R_0, the reference density ρ_0^*, the reference free energy Ψ_0^* sometimes also referred to as attractor stimulus and the two exponents n and m.

4.2. Material motion problem

In complete duality, the free energy density Ψ_t of the material motion problem can be represented as $\Psi_t = \rho_t\Psi$. Within the material motion context, the free energy can be expressed in terms of the reference density ρ_0, the material motion deformation gradient $\boldsymbol{f}$ and the material placements $\boldsymbol{\Phi}$ as $\Psi = \Psi(\rho_0, \boldsymbol{f}, \boldsymbol{\Phi})$. Its spatial time derivative can thus be expanded as $\mathrm{d}_t\Psi = \mathrm{d}_{\rho_0}\Psi\mathrm{d}_t\rho_0 + \mathrm{d}_{\boldsymbol{f}}\Psi : \mathrm{d}_t\boldsymbol{f} + \partial_{\boldsymbol{\Phi}}\Psi : \mathrm{d}_t\boldsymbol{\Phi}$. With $\mathsf{M}_t\Psi = \Psi\partial_{\boldsymbol{\Phi}}\rho_t + \Psi\mathrm{d}_{\boldsymbol{f}}\rho_t : \mathrm{d}_t\boldsymbol{f}$, the Euler theorem and the restriction to the isothermal case, Eq. (14) reduces to the material motion Clausius–Planck inequality:

$$\begin{aligned}\overline{\mathsf{D}}_t = {} & [\overline{\boldsymbol{\pi}}^t - \rho_t\mathrm{d}_{\boldsymbol{f}}\Psi - \Psi\mathrm{d}_{\boldsymbol{f}}\rho_t] : \mathrm{d}_t\boldsymbol{f} - [\overline{\boldsymbol{B}}_t^{\mathrm{int}} + \rho_t\mathrm{d}_{\rho_0}\Psi\nabla_X\rho_0 + \rho_t\partial_{\boldsymbol{\Phi}}\Psi + \Psi\partial_{\boldsymbol{\Phi}}\rho_t]\cdot\boldsymbol{V} \\ & - [\operatorname{div}\boldsymbol{r} - \mathscr{R}_t]\rho_0\mathrm{d}_{\rho_0}\Psi + [\operatorname{div}\boldsymbol{s} - \mathscr{S}_t]\theta \geqslant 0.\end{aligned} \tag{28}$$

It yields the definition of the material motion momentum flux $\overline{\boldsymbol{\pi}}^t$ and the internal forces $\overline{\boldsymbol{B}}_t^{\mathrm{int}}$

$$\overline{\boldsymbol{\pi}}^t = \rho_t\mathrm{d}_{\boldsymbol{f}}\Psi + \Psi\mathrm{d}_{\boldsymbol{f}}\rho_t, \quad \overline{\boldsymbol{B}}_t^{\mathrm{int}} = -\rho_t\mathrm{d}_{\rho_0}\Psi\nabla_X\rho_0 - \rho_t\partial_{\boldsymbol{\Phi}}\Psi - \Psi\partial_{\boldsymbol{\Phi}}\rho_t, \tag{29}$$

and the reduced dissipation inequalitiy:

$$\overline{\mathsf{D}}_t = -[\operatorname{div}\boldsymbol{r} - \mathscr{R}_t]\rho_0\mathrm{d}_{\rho_0}\Psi + [\operatorname{div}\boldsymbol{s} - \mathscr{S}_t]\theta \geqslant 0. \tag{30}$$

Note that the evaluation of the material motion version of the Clausius–Planck inequality does not provide any independent new results. The resulting reduced dissipation inequality is thus nothing but a weighted version of its spatial motion counterpart weighted by the Jacobian j.

Remark 4.1 (*Spatial vs. material quantities*). The vector-valued balance of momentum of the material motion problem can be understood as a complete pull back of the spatial motion momentum balance onto the material manifold, see e.g. Maugin [32]. Thereby, we have to make use of the fundamental relation between the material and the spatial momentum density $\boldsymbol{P} = -\boldsymbol{F}^t\cdot\boldsymbol{p}$. Moreover, we apply the kinematic compatibility condition as $\nabla_X\boldsymbol{F}^t : \overline{\boldsymbol{\Pi}}^t = \overline{\boldsymbol{\Pi}}^t : \nabla_X\boldsymbol{F}$ with $\overline{\boldsymbol{\Pi}}_D^t = \overline{\boldsymbol{\Pi}}^t$ and make use of the existence of a potential for the momentum flux $\overline{\boldsymbol{\Pi}}^t$, such that $\overline{\boldsymbol{\Pi}}^t = \rho_0\partial_{\boldsymbol{F}}\Psi$. Finally, the relation between the spatial and the material motion momentum flux follows as

$$\overline{\boldsymbol{\pi}}_d^t = -j\boldsymbol{F}^t\cdot\overline{\boldsymbol{\Pi}}_D^t\cdot\boldsymbol{F}^t + j\rho_0[\Psi - K]\boldsymbol{F}^t - j\rho_0\boldsymbol{P}\otimes\boldsymbol{v}, \tag{31}$$

while the momentum sources are related via the following transformation:

$$\overline{\boldsymbol{B}}_t = -j\boldsymbol{F}^t\cdot\overline{\boldsymbol{b}}_0 - j\rho_0\mathrm{d}_{\rho_0}\Psi\nabla_X\rho_0 - j\rho_0\partial_{\boldsymbol{\Phi}}[\Psi - K] - j\Psi\partial_{\boldsymbol{\Phi}}\rho_0. \tag{32}$$

For a detailed derivation of the above relations we refer to Kuhl and Steinmann [25], where the complete pull back of the spatial motion momentum balance onto the material manifold is illustrated in detail for open system thermodynamics.

Remark 4.2 (*Constitutive equations for the mass flux and source*). Unlike the reduced momentum fluxes $\overline{\boldsymbol{\Pi}}^t$ and $\overline{\boldsymbol{\pi}}^t$ which follow directly from the evaluation of the Clausius–Duhem inequality, the mass flux and source can be defined without any further restrictions. At this stage, the constitutive equations for the mass flux $\boldsymbol{R}$ and the mass source $\mathscr{R}_0$ are introduced by mere reasoning. However, it will turn out later, that the proposed constitutive equations coincide with the conclusions that can be drawn from the analysis of the material force method.

Remark 4.3 (*Role of the mass flux in biomechanical problems*). Recall that in hard tissue mechanics, particularly in the functional adaption of bones, bone material is typically dissolved by cells that return it to the circulation. A different type of cells would then be able to extract it from the circulation at another location of the body to generate new bone where needed. Consequently, matter is likely to move long distances in hard tissue mechanics. The influence of the mass flux $\boldsymbol{R}$ would thus be less pronounced. In soft tissue mechanics, however, we might encounter real diffusive processes of matter travelling short distances. A typical example is the wound healing of skin where surface tension drives the migration of cells to close the open wound, see e.g. Kuhl and Steinmann [28] or Gambarotta et al. [12].

5. Forces and virtual work

In the present section, we shall highlight the formal duality of the notions of spatial and material forces by comparing the reduced momentum balance in its spatial and material format. For further considerations, it proves convenient to recast both, the mass and the momentum balance, in their weak or rather variational form. Later on, these weak forms will serve as fundamental basis for the finite element discretization.

5.1. Spatial motion problem

First, we shall recast the balance of mass and momentum (17) into their residual format and evaluate those over an arbitrary subdomain $\mathscr{B}_0$,

$$\begin{aligned} r^{\rho}(\rho_0,\boldsymbol{\varphi}) &= f^{\rho}_{\text{dyn}} - f^{\rho}_{\text{sur}} - f^{\rho}_{\text{vol}} = 0, \\ \boldsymbol{r}^{\varphi}(\rho_0,\boldsymbol{\varphi}) &= \boldsymbol{f}^{\varphi}_{\text{dyn}} - \boldsymbol{f}^{\varphi}_{\text{sur}} - \boldsymbol{f}^{\varphi}_{\text{vol}} = \boldsymbol{0}, \end{aligned} \tag{33}$$

whereby the dynamic, the surface and the volume contributions can be expressed in the following form:

$$\begin{aligned} f^{\rho}_{\text{dyn}} &= \int_{\mathscr{B}_0} \mathrm{D}_t \rho_0 \,\mathrm{d}V, \quad f^{\rho}_{\text{sur}} = \int_{\partial\mathscr{B}_0} \boldsymbol{R}\cdot\boldsymbol{N}\,\mathrm{d}A, \quad f^{\rho}_{\text{vol}} = \int_{\mathscr{B}_0} \mathscr{R}_0\,\mathrm{d}V, \\ \boldsymbol{f}^{\varphi}_{\text{dyn}} &= \int_{\mathscr{B}_0} \rho_0 \mathrm{D}_t\boldsymbol{p}\,\mathrm{d}V, \quad \boldsymbol{f}^{\varphi}_{\text{sur}} = \int_{\partial\mathscr{B}_0} \overline{\boldsymbol{\Pi}}^t_D\cdot\boldsymbol{N}\,\mathrm{d}A, \quad \boldsymbol{f}^{\varphi}_{\text{vol}} = \int_{\mathscr{B}_0} \overline{\boldsymbol{b}}_0\,\mathrm{d}V. \end{aligned} \tag{34}$$

For the density problem $(33)_1$, the boundary $\partial\mathscr{B}_0$ is decomposed into disjoint parts $\partial\mathscr{B}^{\rho}_0$ and $\partial\mathscr{B}^{r}_0$. For the deformation problem, the equivalent decomposition renders the disjoint boundary contributions $\partial\mathscr{B}^{\varphi}_0$ and $\partial\mathscr{B}^{t}_0$:

$$\begin{aligned} \partial\mathscr{B}^{\rho}_0 \cup \partial\mathscr{B}^{r}_0 &= \partial\mathscr{B}_0, \quad \partial\mathscr{B}^{\rho}_0 \cap \partial\mathscr{B}^{r}_0 = \emptyset, \\ \partial\mathscr{B}^{\varphi}_0 \cup \partial\mathscr{B}^{t}_0 &= \partial\mathscr{B}_0, \quad \partial\mathscr{B}^{\varphi}_0 \cap \partial\mathscr{B}^{t}_0 = \emptyset. \end{aligned} \tag{35}$$

Standard Dirichlet boundary conditions for the density ρ_0 and the deformation $\boldsymbol{\varphi}$ can be prescribed on $\partial\mathscr{B}^{\rho}_0$ and $\partial\mathscr{B}^{\varphi}_0$. On the Neumann boundary $\partial\mathscr{B}^{r}_0$ and $\partial\mathscr{B}^{t}_0$, the normal projection of the mass flux $\boldsymbol{R}$ and the

reduced momentum source $\overline{\boldsymbol{\Pi}}^t_D$ are typically expressed in terms of the classical closed system terms r^{closed} and $\boldsymbol{t}^{\text{closed}}$ and the possible non–standard open system contributions $\overline{r}^{\text{open}}$ and $\overline{\boldsymbol{t}}^{\text{open}}$:

$$\begin{aligned} &\rho_0 = \overline{\rho}_0 \quad \text{on } \partial\mathscr{B}_0^\rho, \quad \boldsymbol{R}(\rho_0,\boldsymbol{\varphi})\cdot\boldsymbol{N} = r^{\text{closed}} + \overline{r}^{\text{open}} \quad \text{on } \partial\mathscr{B}_0^r, \\ &\boldsymbol{\varphi} = \overline{\boldsymbol{\varphi}} \quad \text{on } \partial\mathscr{B}_0^\varphi, \quad \overline{\boldsymbol{\Pi}}^t_D(\rho_0,\boldsymbol{\varphi})\cdot\boldsymbol{N} = \boldsymbol{t}^{\text{closed}} + \overline{\boldsymbol{t}}^{\text{open}} \quad \text{on } \partial\mathscr{B}_0^t. \end{aligned} \tag{36}$$

The weak forms corresponding to Eqs. (33) can be derived by testing the set of equations with the scalar-valued test function ϱ and the vector-valued test function $\boldsymbol{w}$, respectively. Under the necessary smoothness and boundary assumptions, we straightly obtain the familiar weak forms of the spatial balance of mass and momentum:

$$\begin{aligned} &\mathfrak{g}^\rho(\varrho;\rho_0,\boldsymbol{\varphi}) = w^\rho_{\text{dyn}} + w^\rho_{\text{int}} - w^\rho_{\text{sur}} - w^\rho_{\text{vol}} = 0 \quad \forall\varrho \quad \text{in } H^0_1(\mathscr{B}_0), \\ &\mathfrak{g}^\varphi(\boldsymbol{w};\rho_0,\boldsymbol{\varphi}) = w^\varphi_{\text{dyn}} + w^\varphi_{\text{int}} - w^\varphi_{\text{sur}} - w^\varphi_{\text{vol}} = 0 \quad \forall\boldsymbol{w} \quad \text{in } H^0_1(\mathscr{B}_0). \end{aligned} \tag{37}$$

The dynamic, the internal, the surface and the volume term related to the balance of mass $(37)_1$ are given in the following form:

$$\begin{aligned} &w^\rho_{\text{dyn}} = \int_{\mathscr{B}_0} \varrho \mathrm{D}_t\rho_0 \,\mathrm{d}V, \quad w^\rho_{\text{int}} = \int_{\mathscr{B}_0} \nabla_X\varrho\cdot\boldsymbol{R}\,\mathrm{d}V, \\ &w^\rho_{\text{sur}} = \int_{\partial\mathscr{B}_0} \varrho\boldsymbol{R}\cdot\boldsymbol{N}\,\mathrm{d}A, \quad w^\rho_{\text{vol}} = \int_{\mathscr{B}_0} \varrho\mathscr{R}_0\,\mathrm{d}V. \end{aligned} \tag{38}$$

By interpreting the test function $\boldsymbol{w}$ as the spatial virtual displacement $\boldsymbol{w} = \delta\boldsymbol{\varphi}$, Eq. $(37)_2$ can be identified as the virtual work expression of the spatial motion problem. The dynamic and the internal virtual work w^φ_{dyn} and w^φ_{int} and the corresponding surface and volume contributions w^φ_{sur} and w^φ_{vol} thus take the familiar form known from classical closed system mechanics:

$$\begin{aligned} &w^\varphi_{\text{dyn}} = \int_{\mathscr{B}_0} \boldsymbol{w}\cdot\rho_0\mathrm{D}_t\boldsymbol{p}\,\mathrm{d}V, \quad w^\varphi_{\text{int}} = \int_{\mathscr{B}_0} \nabla_X\boldsymbol{w} : \overline{\boldsymbol{\Pi}}^t_D\,\mathrm{d}V, \\ &w^\varphi_{\text{sur}} = \int_{\partial\mathscr{B}_0} \boldsymbol{w}\cdot\overline{\boldsymbol{\Pi}}^t_D\cdot\boldsymbol{N}\,\mathrm{d}A, \quad w^\varphi_{\text{vol}} = \int_{\mathscr{B}_0} \boldsymbol{w}\cdot\overline{\boldsymbol{b}}_0\,\mathrm{d}V. \end{aligned} \tag{39}$$

5.2. Material motion problem

In complete duality to the spatial motion case, we can introduce the residual format of the balance of mass and momentum (18) for the material motion problem,

$$\begin{aligned} &R^\rho = F^\rho_{\text{dyn}} - F^\rho_{\text{sur}} - F^\rho_{\text{vol}} = 0, \\ &\boldsymbol{R}^\Phi = \boldsymbol{F}^\Phi_{\text{dyn}} - \boldsymbol{F}^\Phi_{\text{sur}} - \boldsymbol{F}^\Phi_{\text{vol}} = \boldsymbol{0}, \end{aligned} \tag{40}$$

with the dynamic, surface and volume contributions defined on the arbitrary spatial subdomain $\mathscr{B}_t$:

$$\begin{aligned} &F^\rho_{\text{dyn}} = \int_{\mathscr{B}_t} j\mathrm{D}_t\rho_0\,\mathrm{d}v, \quad F^\rho_{\text{sur}} = \int_{\partial\mathscr{B}_t} \boldsymbol{r}\cdot\boldsymbol{n}\mathrm{d}a, \quad F^\rho_{\text{vol}} = \int_{\mathscr{B}_t} \mathscr{R}_t\,\mathrm{d}v, \\ &\boldsymbol{F}^\Phi_{\text{dyn}} = \int_{\mathscr{B}_t} \rho_t\mathrm{D}_t\boldsymbol{P}\,\mathrm{d}v, \quad \boldsymbol{F}^\Phi_{\text{sur}} = \int_{\partial\mathscr{B}_t} \overline{\boldsymbol{\pi}}^t_D\cdot\boldsymbol{n}\mathrm{d}a, \quad \boldsymbol{F}^\Phi_{\text{vol}} = \int_{\mathscr{B}_t} \overline{\boldsymbol{B}}_t\,\mathrm{d}v. \end{aligned} \tag{41}$$

To illustrate the duality with the spatial motion problem, we can formally introduce Dirichlet and Neumann boundary conditions on $\partial\mathscr{B}^\rho_t$ and $\partial\mathscr{B}^R_t$ for the density problem and on $\partial\mathscr{B}^\Phi_t$ and $\partial\mathscr{B}^T_t$ for the deformation problem, whereby

$$\begin{aligned} &\partial\mathscr{B}_t^{\rho} \cup \partial\mathscr{B}_t^{R} = \partial\mathscr{B}_t, \quad \partial\mathscr{B}_t^{\rho} \cap \partial\mathscr{B}_t^{R} = \emptyset, \\ &\partial\mathscr{B}_t^{\Phi} \cup \partial\mathscr{B}_t^{T} = \partial\mathscr{B}_t, \quad \partial\mathscr{B}_t^{\Phi} \cap \partial\mathscr{B}_t^{T} = \emptyset, \end{aligned} \tag{42}$$

illustrates the decomposition of the spatial boundary into disjoint parts with the following formally introduced boundary conditions:

$$\begin{aligned} &\rho_0 = \overline{\rho}_0 \quad \text{on } \partial\mathscr{B}_t^{\rho}, \quad \boldsymbol{r}(\rho_0, \boldsymbol{\Phi}) \cdot \boldsymbol{n} = R^{\text{closed}} + \overline{R}^{\text{open}} \quad \text{on } \partial\mathscr{B}_t^{R}, \\ &\boldsymbol{\Phi} = \overline{\boldsymbol{\Phi}} \quad \text{on } \partial\mathscr{B}_t^{\Phi}, \quad \overline{\boldsymbol{\pi}}_D^t(\rho_0, \boldsymbol{\Phi}) \cdot \boldsymbol{n} = \boldsymbol{T}^{\text{closed}} + \overline{\boldsymbol{T}}^{\text{open}} \quad \text{on } \partial\mathscr{B}_t^{T}. \end{aligned} \tag{43}$$

By testing the point-wise statements of the material mass and momentum balance (10) and (11) with the scalar- and vector-valued test functions ϱ and $\boldsymbol{W}$, we obtain the related weak forms:

$$\begin{aligned} &\mathfrak{G}^{\rho}(\varrho; \rho_0, \boldsymbol{\Phi}) = W_{\text{dyn}}^{\rho} + W_{\text{int}}^{\rho} - W_{\text{sur}}^{\rho} - W_{\text{vol}}^{\rho} = 0 \quad \forall \varrho \quad \text{in } H_1^0(\mathscr{B}_t), \\ &\mathfrak{G}^{\Phi}(\boldsymbol{W}; \rho_0, \boldsymbol{\Phi}) = W_{\text{dyn}}^{\Phi} + W_{\text{int}}^{\Phi} - W_{\text{sur}}^{\Phi} - W_{\text{vol}}^{\Phi} = 0 \quad \forall \boldsymbol{W} \quad \text{in } H_1^0(\mathscr{B}_t). \end{aligned} \tag{44}$$

Thereby, the dynamic, the internal, the surface and the volume contribution to the weak form of the mass balance $(44)_1$ can be expressed in the following form:

$$\begin{aligned} &W_{\text{dyn}}^{\rho} = \int_{\mathscr{B}_t} \varrho j \mathrm{D}_t \rho_0 \, \mathrm{d}v, \quad W_{\text{int}}^{\rho} = \int_{\mathscr{B}_t} \nabla_x \varrho \cdot \boldsymbol{r} \, \mathrm{d}v, \\ &W_{\text{sur}}^{\rho} = \int_{\partial\mathscr{B}_t} \varrho \boldsymbol{r} \cdot \boldsymbol{n} \, \mathrm{d}a, \quad W_{\text{vol}}^{\rho} = \int_{\mathscr{B}_t} \varrho \mathscr{R}_t \, \mathrm{d}v. \end{aligned} \tag{45}$$

Note that by interpreting the test function $\boldsymbol{W}$ as the material virtual displacement $\boldsymbol{W} = \delta\boldsymbol{\Phi}$, Eq. $(44)_2$ can be interpreted as the material counterpart of the classical virtual work expression $(37)_2$. Accordingly, W_{dyn}^{Φ} and W_{int}^{Φ} denote the dynamic and the internal virtual work, while W_{sur}^{Φ} and W_{vol}^{Φ} are the corresponding surface and volume contributions:

$$\begin{aligned} &W_{\text{dyn}}^{\Phi} = \int_{\mathscr{B}_t} \boldsymbol{W} \cdot \rho_t \mathrm{D}_t \boldsymbol{P} \, \mathrm{d}v, \quad W_{\text{int}}^{\Phi} = \int_{\mathscr{B}_t} \nabla_x \boldsymbol{W} : \overline{\boldsymbol{\pi}}_D^t \, \mathrm{d}v, \\ &W_{\text{sur}}^{\Phi} = \int_{\partial\mathscr{B}_t} \boldsymbol{W} \cdot \overline{\boldsymbol{\pi}}_D^t \cdot \boldsymbol{n} \, \mathrm{d}a, \quad W_{\text{vol}}^{\Phi} = \int_{\mathscr{B}_t} \boldsymbol{W} \cdot \overline{\boldsymbol{B}}_t \, \mathrm{d}v. \end{aligned} \tag{46}$$

Remark 5.1. Note that Eqs. $(34)_2$ define the different contributions to the spatial forces $\boldsymbol{f}^{\varphi}$ representing the traditional forces in the sense of Newton. They are generated by variations relative to the ambient space at fixed material position $\boldsymbol{X}$. On the contrary, Eq. $(41)_2$ define material forces $\boldsymbol{F}^{\Phi}$ in the sense of Eshelby. Material forces are generated by variations relative to the ambient material at fixed spatial position $\boldsymbol{x}$ and thus represent important measures in the mechanics of material inhomogeneities.

Remark 5.2. Recall that for the spatial motion case, the surface and the volume terms of the weak forms (37), namely w_{sur}^{ρ} and w_{vol}^{ρ} for the density problem and w_{sur}^{φ} and w_{vol}^{φ} for the deformation problem are usually given while the density ρ_0 and the spatial motion $\boldsymbol{\varphi}$ furnish the primary unknowns. Once the spatial motion problem is solved, the dynamic term W_{dyn}^{Φ}, the internal virtual work W_{int}^{Φ} and the volume contribution W_{vol}^{Φ} to the material momentum balance can be computed directly. Correspondingly, the material surface forces $\boldsymbol{F}_{\text{sur}}^{\Phi}$ furnish the unknown of the computational analysis, which has been advocated as "material force method" by Steinmann et al. [43].

Remark 5.3. Note that the scalar-valued test function ϱ testing the balance of mass is identical for the spatial and the material motion problem. The weak forms of the reduced momentum balance, i.e. the virtual work expressions of the spatial and the material motion problem $(37)_2$ and $(44)_2$ can be transformed into one another in a straightforward way by making use of the fundamental relations $\boldsymbol{w} = -\boldsymbol{W} \cdot \boldsymbol{F}^t$ and $\boldsymbol{W} = -\boldsymbol{w} \cdot \boldsymbol{f}^t$ between the spatial and the material virtual displacements $\boldsymbol{w} = \delta\boldsymbol{\varphi}$ and $\boldsymbol{W} = \delta\boldsymbol{\Phi}$.

6. Discretization

Eqs. (37) and (44) represent the continuous version of the spatial and the material initial boundary value problem of open system mechanics. Following the classical approach, we shall first perform a temporal discretization followed by a discretization in space to obtain the fully discrete spatial and material set of governing equations. For the temporal discretization, consider a partition of the time interval of interest $\mathscr{T}$

$$\mathscr{T} = \bigcup_{n=0}^{n_{\text{step}}-1} [t_n, t_{n+1}], \tag{47}$$

and focus on the typical subinterval $[t_n, t_{n+1}]$ whereby $\Delta t = t_{n+1} - t_n$ denotes the corresponding actual time increment. The primary unknowns $\rho_{0\,n}$ and $\boldsymbol{\varphi}_n$ for the spatial motion problem and $\rho_{0\,n}$ and $\boldsymbol{\Phi}_n$ for the material motion problem and all derivable quantities are assumed to be known at t_n. Without loss of generality, we shall apply the classical implicit Euler backward time integration scheme to advance the solution in time from the known time step t_n to the actual time step t_{n+1}. Thereby, the first order material time derivatives of the density and the mass specific momentum density are approximated as

$$\begin{aligned} \mathrm{D}_t\rho_0 &= \frac{1}{\Delta t}[\rho_{0\,n+1} - \rho_{0\,n}], \quad \mathrm{D}_t\boldsymbol{p} = \frac{1}{\Delta t}[\boldsymbol{p}_{n+1} - \boldsymbol{p}_n], \\ \mathrm{D}_t\rho_0 &= \frac{1}{\Delta t}[\rho_{0\,n+1} - \rho_{0\,n}], \quad \mathrm{D}_t\boldsymbol{P} = \frac{1}{\Delta t}[\boldsymbol{P}_{n+1} - \boldsymbol{P}_n], \end{aligned} \tag{48}$$

for the spatial and the material motion problem, respectively. We can now reformulate the governing equations for the spatial motion problem (37) in terms of the unknowns $\rho_{0\,n+1}$ and $\boldsymbol{\varphi}_{n+1}$:

$$\begin{aligned} \mathfrak{g}^{\rho}_{n+1}(\varrho; \rho_{0\,n+1}, \boldsymbol{\varphi}_{n+1}) &= w^{\rho}_{\text{dyn}} + w^{\rho}_{\text{int}} - w^{\rho}_{\text{sur}} - w^{\rho}_{\text{vol}} = 0 \quad \forall \varrho \quad \text{in } H^0_1(\mathscr{B}_0), \\ \mathfrak{g}^{\varphi}_{n+1}(\boldsymbol{w}; \rho_{0\,n+1}, \boldsymbol{\varphi}_{n+1}) &= w^{\varphi}_{\text{dyn}} + w^{\varphi}_{\text{int}} - w^{\varphi}_{\text{sur}} - w^{\varphi}_{\text{vol}} = 0 \quad \forall \boldsymbol{w} \quad \text{in } H^0_1(\mathscr{B}_0). \end{aligned} \tag{49}$$

Accordingly, the governing equations for the material motion problem (44) can be expressed in terms of $\rho_{0\,n+1}$ and $\boldsymbol{\Phi}_{n+1}$:

$$\begin{aligned} \mathfrak{G}^{\rho}_{n+1}(\varrho; \rho_{0\,n+1}, \boldsymbol{\Phi}_{n+1}) &= W^{\rho}_{\text{dyn}} + W^{\rho}_{\text{int}} - W^{\rho}_{\text{sur}} - W^{\rho}_{\text{vol}} = 0 \quad \forall \varrho \quad \text{in } H^0_1(\mathscr{B}_t), \\ \mathfrak{G}^{\Phi}_{n+1}(\boldsymbol{W}; \rho_{0\,n+1}, \boldsymbol{\Phi}_{n+1}) &= W^{\Phi}_{\text{dyn}} + W^{\Phi}_{\text{int}} - W^{\Phi}_{\text{sur}} - W^{\Phi}_{\text{vol}} = 0 \quad \forall \boldsymbol{W} \quad \text{in } H^0_1(\mathscr{B}_t). \end{aligned} \tag{50}$$

Next, the semi-discrete sets of governing Eqs. (49) and (50) will be discretized in space with the finite element method.

6.1. Spatial motion problem

Let $\mathscr{B}_0$ denote the region occupied by the reference configuration of a solid continuum body at time $t = t_0$. In the spirit of the finite element method, this reference domain is discretized in n_{el} elements $\mathscr{B}^e_0$. The underlying geometry $\boldsymbol{X}$ is interpolated elementwise by the shape functions N^i_X in terms of the discrete node point positions $\boldsymbol{X}_i$ of the $i = 1, \ldots, n_{\text{en}}$ element nodes:

$$\mathscr{B}_0 = \bigcup_{e=1}^{n_{\text{el}}} \mathscr{B}_0^e \quad \boldsymbol{X}^h|_{\mathscr{B}_0^e} = \sum_{I=1}^{n_{\text{nod}}} N_X^i \boldsymbol{X}_i. \tag{51}$$

Following the isoparametric concept, the unknowns ρ_0 and $\boldsymbol{\varphi}$ are interpolated on the element level with the same shape functions N_ρ^i and N_φ^j as the element geometry $\boldsymbol{X}$. Similar shape functions are applied to interpolate the test functions ϱ and $\boldsymbol{w}$ according to the classical Bubnov–Galerkin technique:

$$\begin{aligned} \varrho^h|_{\mathscr{B}_0^e} &= \sum_{i=1}^{n_{\text{en}}} N_\rho^i \varrho_i \in H_1^0(\mathscr{B}_0), \quad \rho_0^h|_{\mathscr{B}_0^e} = \sum_{k=1}^{n_{\text{en}}} N_\rho^k \rho_k \in H_1(\mathscr{B}_0), \\ \boldsymbol{w}^h|_{\mathscr{B}_0^e} &= \sum_{j=1}^{n_{\text{en}}} N_\varphi^j \boldsymbol{w}_j \in H_1^0(\mathscr{B}_0), \quad \boldsymbol{\varphi}^h|_{\mathscr{B}_0^e} = \sum_{l=1}^{n_{\text{en}}} N_\varphi^l \boldsymbol{\varphi}_l \in H_1(\mathscr{B}_0). \end{aligned} \tag{52}$$

The related gradients of the test functions $\nabla_X \varrho^h$ and $\nabla_X \boldsymbol{w}^h$ and the gradients of the primary unknowns $\nabla_X \rho_0^h$ and $\nabla_X \boldsymbol{\varphi}^h$ thus take the following elementwise interpolation,

$$\begin{aligned} \nabla_X \varrho^h|_{\mathscr{B}_0^e} &= \sum_{i=1}^{n_{\text{en}}} \varrho_i \nabla_X N_\rho^i, \quad \nabla_X \rho_0^h|_{\mathscr{B}_0^e} = \sum_{k=1}^{n_{\text{en}}} \rho_k \nabla_X N_\rho^k, \\ \nabla_X \boldsymbol{w}^h|_{\mathscr{B}_0^e} &= \sum_{j=1}^{n_{\text{en}}} \boldsymbol{w}_j \otimes \nabla_X N_\varphi^j, \quad \nabla_X \boldsymbol{\varphi}^h|_{\mathscr{B}_0^e} = \sum_{l=1}^{n_{\text{en}}} \boldsymbol{\varphi}_l \otimes \nabla_X N_\varphi^l, \end{aligned} \tag{53}$$

whereby $\nabla_X \boldsymbol{\varphi}^h|_{\mathscr{B}_0^e}$ in particular denotes the discrete spatial deformation gradient as $\boldsymbol{F}^h|_{\mathscr{B}_0^e} = \nabla_X \boldsymbol{\varphi}^h|_{\mathscr{B}_0^e}$. With the above suggested discretizations in time and space, the discrete algorithmic balance of mass and momentum of the spatial motion problem can be expressed as

$$\begin{aligned} r_I^{\rho h}(\rho_{0\,n+1}^h, \boldsymbol{\varphi}_{n+1}^h) &= f_{\text{dyn}\,I}^{\rho h} + f_{\text{int}\,I}^{\rho h} - f_{\text{sur}\,I}^{\rho h} - f_{\text{vol}\,I}^{\rho h} = 0 \quad \forall I = 1, n_{\text{np}}, \\ \boldsymbol{r}_J^{\varphi h}(\rho_{0\,n+1}^h, \boldsymbol{\varphi}_{n+1}^h) &= \boldsymbol{f}_{\text{dyn}\,J}^{\varphi h} + \boldsymbol{f}_{\text{int}\,J}^{\varphi h} - \boldsymbol{f}_{\text{sur}\,J}^{\varphi h} - \boldsymbol{f}_{\text{vol}\,J}^{\varphi h} = \boldsymbol{0} \quad \forall J = 1, n_{\text{np}}, \end{aligned} \tag{54}$$

with the dynamic, the internal, the surface and the volume contribution of the balance of mass expanding to the following expressions:

$$\begin{aligned} f_{\text{dyn}\,I}^{\rho h} &= \mathop{\mathbf{A}}_{e=1}^{n_{\text{el}}} \int_{\mathscr{B}_0^e} N_\rho^i \frac{\rho_{0\,n+1} - \rho_{0\,n}}{\Delta t}\, \mathrm{d}V, \quad f_{\text{int}\,I}^{\rho h} = \mathop{\mathbf{A}}_{e=1}^{n_{\text{el}}} \int_{\mathscr{B}_0^e} \nabla_X N_\rho^i \cdot \boldsymbol{R}_{n+1}\, \mathrm{d}V, \\ f_{\text{sur}\,I}^{\rho h} &= \mathop{\mathbf{A}}_{e=1}^{n_{\text{el}}} \int_{\partial \mathscr{B}_0^{er}} N_\rho^i [r_{n+1}^{\text{closed}} + \overline{r}_{n+1}^{\text{open}}]\, \mathrm{d}A, \quad f_{\text{vol}\,I}^{\rho h} = \mathop{\mathbf{A}}_{e=1}^{n_{\text{el}}} \int_{\mathscr{B}_0^e} N_\rho^i \mathscr{R}_{0\,n+1}\, \mathrm{d}V. \end{aligned} \tag{55}$$

The corresponding discrete inertia forces, the internal forces, the surface forces and the volume forces take the following format,

$$\begin{aligned} \boldsymbol{f}_{\text{dyn}\,J}^{\varphi h} &= \mathop{\mathbf{A}}_{e=1}^{n_{\text{el}}} \int_{\mathscr{B}_0^e} N_\varphi^j \rho_0 \frac{\boldsymbol{p}_{n+1} - \boldsymbol{p}_n}{\Delta t}\, \mathrm{d}V, \quad \boldsymbol{f}_{\text{int}\,J}^{\varphi h} = \mathop{\mathbf{A}}_{e=1}^{n_{\text{el}}} \int_{\mathscr{B}_0^e} \nabla_X N_\varphi^j \cdot \overline{\boldsymbol{\Pi}}_{D\,n+1}\, \mathrm{d}V, \\ \boldsymbol{f}_{\text{sur}\,J}^{\varphi h} &= \mathop{\mathbf{A}}_{e=1}^{n_{\text{el}}} \int_{\partial \mathscr{B}_0^{te}} N_\varphi^j [\boldsymbol{t}_{n+1}^{\text{closed}} + \overline{\boldsymbol{t}}_{n+1}^{\text{open}}]\, \mathrm{d}A, \quad \boldsymbol{f}_{\text{vol}\,J}^{\varphi h} = \mathop{\mathbf{A}}_{e=1}^{n_{\text{el}}} \int_{\mathscr{B}_0^e} N_\varphi^j \overline{\boldsymbol{b}}_{0\,n+1}\, \mathrm{d}V, \end{aligned} \tag{56}$$

with the understanding that the operator $\mathbf{A}$ denotes the assembly over all $e = 1, n_{\text{el}}$ element forces at the $i, j = 1, n_{\text{en}}$ element nodes to the global node point forces at all $I, J = 1, n_{\text{np}}$ global node points. Eqs. (54) represent the coupled non-linear set of governing equations which is suggested to be solved in a monolithic sense. The corresponding solution procedure in terms of the incremental iterative Newton–Raphson scheme is illustrated in the Appendix A, see also Kuhl and Steinmann [26]. It is worth noting, that the discrete spatial surface forces acting on the global node points can be calculated as

$$\boldsymbol{f}^{\varphi h}_{\mathrm{sur}\,J} = \mathop{\mathsf{A}}_{e=1}^{n_{\mathrm{el}}} \int_{\mathscr{B}^e_0} N^j_\varphi \rho_0 \frac{\boldsymbol{p}_{n+1} - \boldsymbol{p}_n}{\Delta t} + \nabla_X N^j_\varphi \cdot \overline{\boldsymbol{\Pi}}_{D\,n+1} - N^j_\varphi \overline{\boldsymbol{b}}_{0\,n+1}\,\mathrm{d}V, \tag{57}$$

and are thus energetically conjugate to spatial variations of the node point positions.

6.2. Material motion problem

For the material motion problem, we discretize the domain of interest $\mathscr{B}_t$ in n_{el} elements $\mathscr{B}^e_t$. The geometry $\boldsymbol{x}$ of each element is interpolated from the $i = 1, \ldots, n_{\mathrm{en}}$ node point positions $\boldsymbol{x}_i$ by the shape functions N^i_x:

$$\mathscr{B}_t = \bigcup_{e=1}^{n_{\mathrm{el}}} \mathscr{B}^e_t \quad \boldsymbol{x}^h|_{\mathscr{B}^e_t} = \sum_{I=1}^{n_{\mathrm{nod}}} N^i_x \boldsymbol{x}_i. \tag{58}$$

Again, we shall interpolate the primary unknowns ρ_0 and $\boldsymbol{\Phi}$ with the same shape functions N^i_ρ and $N^j_{\boldsymbol{\Phi}}$ as the element geometry $\boldsymbol{x}$ by making use of the isoparametric concept. Following the classical Bubnov–Galerkin technique, the test functions ϱ and $\boldsymbol{W}$ are discretized with the same shape functions N^i_ρ and $N^j_{\boldsymbol{\Phi}}$:

$$\begin{aligned} &\varrho^h|_{\mathscr{B}^e_t} = \sum_{i=1}^{n_{\mathrm{en}}} N^i_\rho \varrho_i \in H^0_1(\mathscr{B}_t), \quad \rho^h_0|_{\mathscr{B}^e_t} = \sum_{k=1}^{n_{\mathrm{en}}} N^k_\rho \rho_k \in H_1(\mathscr{B}_t), \\ &\boldsymbol{W}^h|_{\mathscr{B}^e_t} = \sum_{j=1}^{n_{\mathrm{en}}} N^j_\varphi \boldsymbol{W}_j \in H^0_1(\mathscr{B}_t), \quad \boldsymbol{\Phi}^h|_{\mathscr{B}^e_t} = \sum_{l=1}^{n_{\mathrm{en}}} N^l_{\boldsymbol{\Phi}} \boldsymbol{\Phi}_l \in H_1(\mathscr{B}_t). \end{aligned} \tag{59}$$

The discretization of the corresponding gradients of the test functions $\nabla_x \varrho^h$ and $\nabla_x \boldsymbol{W}^h$ and the gradients of the primary unknowns $\nabla_x \rho^h_0$ and $\nabla_x \boldsymbol{\Phi}^h$ thus takes the following representation:

$$\begin{aligned} &\nabla_x \varrho^h|_{\mathscr{B}^e_t} = \sum_{i=1}^{n_{\mathrm{en}}} \varrho_i \nabla_x N^i_\rho, \quad \nabla_x \rho^h_0|_{\mathscr{B}^e_t} = \sum_{k=1}^{n_{\mathrm{en}}} \rho_k \nabla_x N^k_\rho, \\ &\nabla_x \boldsymbol{W}^h|_{\mathscr{B}^e_t} = \sum_{j=1}^{n_{\mathrm{en}}} \boldsymbol{w}_j \otimes \nabla_x N^j_{\boldsymbol{\Phi}}, \quad \nabla_x \boldsymbol{\Phi}^h|_{\mathscr{B}^e_t} = \sum_{l=1}^{n_{\mathrm{en}}} \boldsymbol{\Phi}_l \otimes \nabla_x N^l_{\boldsymbol{\Phi}}. \end{aligned} \tag{60}$$

Note that $\nabla_x \boldsymbol{\Phi}^h$ denotes the discrete material deformation gradient $\boldsymbol{f}^h|_{\mathscr{B}^e_t} = \nabla_x \boldsymbol{\Phi}^h|_{\mathscr{B}^e_t}$. Finally, the discrete algorithmic balance of mass and momentum of the material motion problem can be expressed as follows,

$$\begin{aligned} &R^{\rho h}_I(\rho^h_{0\,n+1}, \boldsymbol{\Phi}^h_{n+1}) = F^{\rho h}_{\mathrm{dyn}\,I} + F^{\rho h}_{\mathrm{int}\,I} - F^{\rho h}_{\mathrm{sur}\,I} - F^{\rho h}_{\mathrm{vol}\,I} = 0 \quad \forall I = 1, n_{\mathrm{np}}, \\ &\boldsymbol{R}^{\Phi h}_J(\rho^h_{0\,n+1}, \boldsymbol{\Phi}^h_{n+1}) = \boldsymbol{F}^{\Phi h}_{\mathrm{dyn}\,J} + \boldsymbol{F}^{\Phi h}_{\mathrm{int}\,J} - \boldsymbol{F}^{\Phi h}_{\mathrm{sur}\,J} - \boldsymbol{F}^{\Phi h}_{\mathrm{vol}\,J} = \boldsymbol{0} \quad \forall J = 1, n_{\mathrm{np}}, \end{aligned} \tag{61}$$

whereby the dynamic, the internal, the surface and the volume contribution of the balance of mass are given in the following form:

$$\begin{aligned} &F^{\rho h}_{\mathrm{dyn}\,I} = \mathop{\mathsf{A}}_{e=1}^{n_{\mathrm{el}}} \int_{\mathscr{B}^e_t} N^i_\rho j \frac{\rho_{0\,n+1} - \rho_{0\,n}}{\Delta t}\,\mathrm{d}v, \quad F^{\rho h}_{\mathrm{int}\,I} = \mathop{\mathsf{A}}_{e=1}^{n_{\mathrm{el}}} \int_{\mathscr{B}^e_t} \nabla_x N^i_\rho \cdot \boldsymbol{r}_{n+1}\,\mathrm{d}v, \\ &F^{\rho h}_{\mathrm{sur}\,I} = \mathop{\mathsf{A}}_{e=1}^{n_{\mathrm{el}}} \int_{\partial\mathscr{B}^e_t} N^i_\rho [R^{\mathrm{closed}}_{n+1} + \overline{R}^{\mathrm{open}}_{n+1}]\mathrm{d}a, \quad F^{\rho h}_{\mathrm{vol}\,I} = \mathop{\mathsf{A}}_{e=1}^{n_{\mathrm{el}}} \int_{\mathscr{B}^e_t} N^i_\rho \mathscr{R}_{t\,n+1}\,\mathrm{d}v. \end{aligned} \tag{62}$$

Moreover, the discrete material inertia forces, the internal forces, the surface forces and the volume forces take the following format:

$$\begin{aligned} &\boldsymbol{F}^{\varphi h}_{\mathrm{dyn}\,J} = \mathop{\mathsf{A}}_{e=1}^{n_{\mathrm{el}}} \int_{\mathscr{B}^e_t} N^j_{\boldsymbol{\Phi}} \rho_t \frac{\boldsymbol{P}_{n+1} - \boldsymbol{P}_n}{\Delta t}\,\mathrm{d}v, \quad \boldsymbol{F}^{\varphi h}_{\mathrm{int}\,J} = \mathop{\mathsf{A}}_{e=1}^{n_{\mathrm{el}}} \int_{\mathscr{B}^e_t} \nabla_x N^j_{\boldsymbol{\Phi}} \cdot \overline{\boldsymbol{\pi}}_{D\,n+1}\,\mathrm{d}v, \\ &\boldsymbol{F}^{\varphi h}_{\mathrm{sur}\,J} = \mathop{\mathsf{A}}_{e=1}^{n_{\mathrm{el}}} \int_{\partial\mathscr{B}^e_t} N^j_{\boldsymbol{\Phi}} [\boldsymbol{T}^{\mathrm{closed}}_{n+1} + \overline{\boldsymbol{T}}^{\mathrm{open}}_{n+1}]\mathrm{d}a, \quad \boldsymbol{F}^{\varphi h}_{\mathrm{vol}\,J} = \mathop{\mathsf{A}}_{e=1}^{n_{\mathrm{el}}} \int_{\mathscr{B}^e_t} N^j_{\boldsymbol{\Phi}} \overline{\boldsymbol{B}}_{t\,n+1}\,\mathrm{d}v. \end{aligned} \tag{63}$$

As a fundamental difference to the spatial motion problem, the Neumann boundary conditions of the material motion problem cannot be considered as given input data. Correspondingly, the discrete material forces acting on the global node points can only be computed in a post processing calculation once the spatial motion problem has been solved. Their definition parallels the definition of the discrete surface forces of the spatial motion problem. The discrete material surface forces

$$\boldsymbol{F}^{\Phi h}_{\mathrm{sur}\,J} = \mathop{\mathsf{A}}_{e=1}^{n_{\mathrm{el}}} \int_{\mathscr{B}^e_t} N^j_{\Phi}\rho_t \frac{\boldsymbol{P}_{n+1}-\boldsymbol{P}_n}{\Delta t} + \nabla_x N^j_{\Phi}\cdot\overline{\boldsymbol{\pi}}_{D\,n+1} - N^j_{\Phi}\overline{\boldsymbol{B}}_{t\,n+1}\,\mathrm{d}v \tag{64}$$

are thus energetically conjugate to material variations of the node point positions.

Remark 6.1. In most practical applications, the time rate of change of the mass and momentum typically differ by orders of magnitude. For biological problems, for example, the momentum balance is therefore considered in a quasi-static sense in order to avoid numerical problems. Consequently, the dynamic contributions which manifest themselves in the $N^j_{\varphi}\rho_0[\boldsymbol{p}_{n+1}-\boldsymbol{p}_n]/\Delta t$ term of Eq. $(56)_1$ and in the $N^j_{\Phi}\rho_t[\boldsymbol{P}_{n+1}-\boldsymbol{P}_n]/\Delta t$ term of Eq. $(63)_1$ are typically neglected. Since the distinction of the different momentum fluxes $\overline{\boldsymbol{\pi}}$, $\overline{\boldsymbol{\pi}}_d$ and $\overline{\boldsymbol{\pi}}_D$ is then no longer necessary, the additional subscripts d and D will be neglected in the sequel.

Remark 6.2 (*Spatial vs. material quantities*). For the quasi-static case, the discrete reduced momentum flux $\overline{\boldsymbol{\pi}}^t_{n+1}$, and the corresponding momentum source $\overline{\boldsymbol{B}}_{t\,n+1}$ that are essentially needed to compute the discrete material node point forces defined in Eq. (64) are related to their spatial motion counterparts through the following transformation formulae:

$$\begin{aligned}
\overline{\boldsymbol{\pi}}^t_{n+1} &= -j\boldsymbol{F}^t_{n+1}\cdot\overline{\boldsymbol{\Pi}}^t_{n+1}\cdot\boldsymbol{F}^t_{n+1} + \rho_{t\,n+1}\Psi_{n+1}\boldsymbol{F}^t_{n+1},\\
\overline{\boldsymbol{B}}_{t\,n+1} &= j\boldsymbol{F}^t_{n+1}\cdot\overline{\boldsymbol{b}}_{0\,n+1} - \rho_{t\,n+1}\partial_{\rho_0}\Psi_{n+1}\nabla_X\rho_{0\,n+1} - \partial_{\boldsymbol{\Phi}}[\rho_{t\,n+1}\Psi_{n+1}].
\end{aligned} \tag{65}$$

7. Examples

The above proposed algorithm for open system mechanics will now be applied to a number of selected examples to illustrate the additional information provided by the material force method. Thereby, we will analyze the evolution of the discrete material node point forces

$$\boldsymbol{F}^{\Phi h}_{\mathrm{sur}\,J} = \boldsymbol{F}^{\Phi h}_{\mathrm{int}\,J} - \boldsymbol{F}^{\Phi h}_{\mathrm{vol}\,J},$$

which can be calculated numerically as the difference between the internal material forces and the material volume forces:

$$\boldsymbol{F}^{\Phi h}_{\mathrm{int}\,J} = \mathop{\mathsf{A}}_{e=1}^{n_{\mathrm{el}}} \int_{\mathscr{B}^e_t} \nabla_x N^j_{\Phi}\cdot\overline{\boldsymbol{\pi}}_{n+1}\,\mathrm{d}v, \quad \boldsymbol{F}^{\Phi h}_{\mathrm{vol}\,J} = \mathop{\mathsf{A}}_{e=1}^{n_{\mathrm{el}}} \int_{\mathscr{B}^e_t} N^j_{\Phi}\overline{\boldsymbol{B}}_{t\,n+1}\,\mathrm{d}v.$$

In what follows, we shall consider the quasi-static, volume force-free case. Accordingly, the discrete material momentum flux $\overline{\boldsymbol{\pi}}_{n+1} = -j\boldsymbol{F}^t_{n+1}\cdot\overline{\boldsymbol{\Pi}}_{n+1}\cdot\boldsymbol{F}^t_{n+1} + \rho_{t\,n+1}\Psi_{n+1}\boldsymbol{F}^t_{n+1}$ and the discrete material momentum source $\overline{\boldsymbol{B}}_{t\,n+1} = -j[n-1]\Psi_{n+1}\nabla_X\rho_{0\,n+1}$ can be computed directly once the spatial problem has been solved. Particular attention is drawn to the discrete material volume forces $\boldsymbol{F}^{\Phi h}_{\mathrm{vol}}$. For the classical application of the material force method to linear or non-linear elastic fracture mechanics, the discrete material volume forces vanish identically in the absence of inhomogeneities and of spatial volume forces with $\overline{\boldsymbol{b}}_{0\,n+1} = \boldsymbol{0}$. However, for the application to open system mechanics considered herein, the discrete material volume forces are

directly proportional to the discrete density gradient $\nabla_X \rho_{0\,n+1}$ and thus indicate the tendency of the material to smooth discontinuities and form a preferably homogeneous density distribution.

7.1. One-dimensional model problem

Let us first consider the academic example of a one-dimensional bar of unit size with Lamé constants of $\lambda = 0$ and $\mu = 0.5$. The specimen has a reference density of $\rho_0^* = 1$ and a reference free energy of $\Psi_0^* = 2$, while the two exponents are chosen to $n = 2$ and $m = 3$. In order to trigger an imperfection, the reference free energy Ψ_0^* has been reduced to $\Psi_0^* = 1$ in an area of 20% of the total specimen length right in the middle of the bar. We apply a constant load of $f = 1$ and simulate 50 time steps of $\Delta t = 0.1$ each, until the density has converged to its final equilibrium distribution. Since most existing models for open systems a priori exclude the influence of mass diffusion, we shall first analyze the model response of a bar for which the mass flux is suppressed as $R_0 = 0$. The resulting density distribution is depicted in Fig. 3.

The discontinuity in the reference free energy Ψ_0^* obviously results in a non-homogeneous density distribution taking maximum values in the middle of the specimen. Typically, the applied $\mathscr{C}^0$-continuous finite element formulation fails to capture the analytical solution of a hat-type density distribution and shows characteristic spurious oscillations close to the discontinuity. To illustrate the tendency of the material to form a homogeneous distribution of matter, we have included the volume contribution to the material forces $\boldsymbol{F}_{\text{vol}}^{\Phi h}$ into Fig. 3. Obviously, the material tends to smooth sharp density contours by flowing in the direction of negative density gradients to achieve an equal concentration throughout the entire bar. This observation coincides with the numerical findings of Müller and Maugin [35], who observed that material forces always try to render the total body more "homogeneous".

Next, we shall therefore allow for the outflux of mass in the direction of the material volume forces $\boldsymbol{F}_{\text{vol}}^{\Phi h}$. A typical example can be found in the healing of wounded skin, where cells tend to crawl into the open wound driven by surface tension in order to render the density distribution as homogeneous as possible and thereby close the wound. The amount of outflux is primarily governed by the mass conduction coefficient R_0 through the constitutive equation for the mass flux (26). Fig. 4 illustrates the resulting density distributions for gradually increasing values of R_0. The increase of the mass conduction coefficient clearly smoothes the density profile and widens the area that is affected by the initial imperfection. The smoother the density distribution, the smaller the related density gradients. The resulting material forces thus decrease with an increasing mass flux. For values of R_0 larger than a critical value, a homogeneous density distribution can be found, compare Fig. 4 (top). As an additional benefit of the incorporation of the mass flux, the spurious oscillations close to the discontinuity that had been present in the flux free simulation of Fig. 3 disappear due the inclusion of the Laplacian term.

In summary, the volume contribution to the material forces $\boldsymbol{F}_{\text{vol}}^{\Phi h}$ can be interpreted as driving force for the movement of material inhomogeneities in the interior of the considered domain. The material force method provides a motivation for the incorporation of the flow of matter along the direction of descending

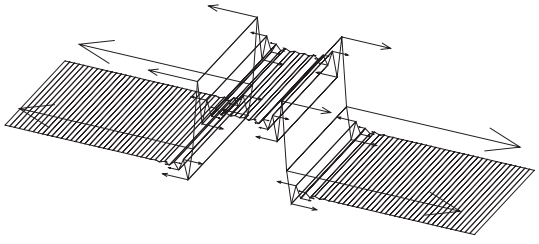

Fig. 3. Density profile ρ_0 and material volume forces $F_{\text{vol}}^{\Phi h}$.

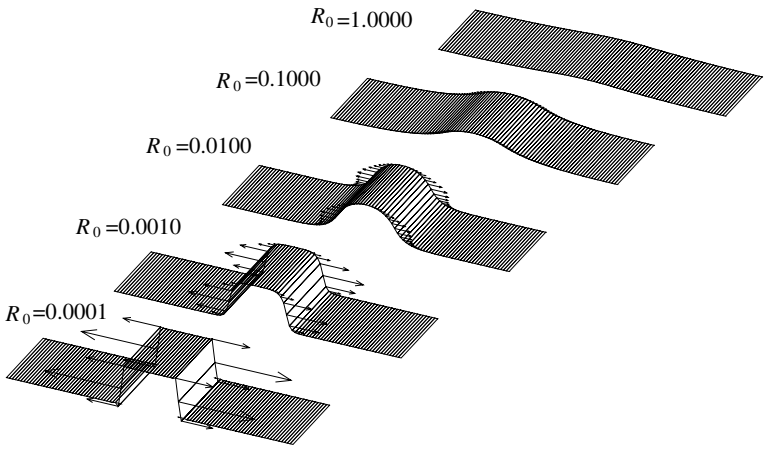

Fig. 4. Density profiles ρ_0 and material volume forces $F_{\text{vol}}^{\Phi h}$ for different R_0.

density gradients. The considered matter thus tends to flow through material with the aim of equilibrating initially unequal density distributions.

7.2. Biomechanics: bone remodeling

The next example, a classical application taken from the field of biomechanics, deals with finding the density distribution in the proxima femur subjected to an average daily loading situation. The underlying geometry and the finite element mesh of 658 four-noded isoparametric elements with 725 nodes is shown in Fig. 5 (left). The system is clamped in the lower left corner and held vertically at the entire lower boundary while the lateral movement of the lower boundary is unconstrained. The bone is loaded by three groups of muscle forces arising during the midstance phase of gait, abduction and adduction, compare Table 1.

In accordance with Carter and Beaupré [4], the Lamé constants take values of $\lambda = 138.89$ and $\mu = 208.33$. Moreover, we choose a reference density of $\rho_0^* = 1.2$, a reference free energy of $\Psi_0^* = 0.01$ and the exponents $n = 2$ and $m = 3$. For the sake of comparability, we neglect the mass flux as $R_0 = 0$. Fig. 5, right shows the resulting density distribution at a final stage of equilibrium after 100 time steps of $\Delta t = 2.0$ each. Dark areas indicate a high density while bone material has been removed locally at light areas. The predicted density pattern clearly coincides with density distributions found experimentally, compare e.g. Wolff [47] and with earlier numerical simulations, see e.g. Carter and Beaupré [4]. Fig. 6 depicts the resulting material surface forces $\boldsymbol{F}_{\text{sur}}^{\Phi h}$ and the corresponding material volume forces $\boldsymbol{F}_{\text{vol}}^{\Phi h}$. Note that for the sake of visualization, the latter has been magnified by a factor four in comparison to the former. Again, the volume contribution depicted on the right indicates the tendency of the material to flow out of areas of high density concentration. When comparing the intensity of the material volume forces with the density distribution of Fig. 5 (right), one typically finds largest forces in areas of highest density gradients, e.g. pointing from the dense media and lateral cortices towards the low density mellulary core in the shaft region. The material surface forces depicted on the lefthand side are about four times larger in their absolute value. On the boundary, material surface forces can be interpreted as a measure of shape sensitivity of the specimen geometry. They thus take larger values at non-smooth surfaces, e.g. close to the medial shaft. In biomechanical applications, the material surface forces on the domain boundary could thus

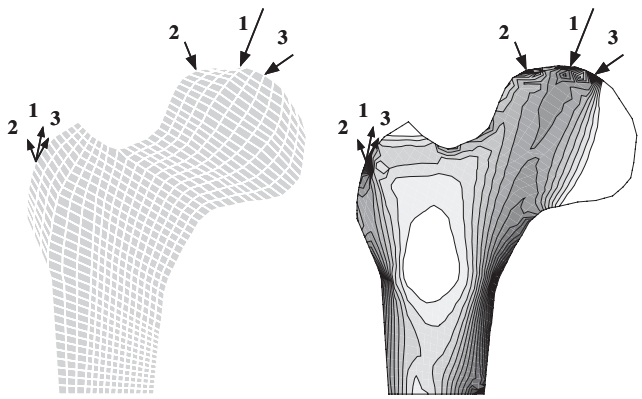

Fig. 5. Proxima femur—finite element mesh and predicted density distribution.

Table 1
Proxima femur—loading conditions

	Type of loading	Value (N)	Direction (°)	Value (N)	Direction (°)
1	Midstance phase of gait	2317	24	703	28
2	Extreme range of abduction	1158	−15	351	−8
3	Extreme range of adduction	1548	56	468	35

be understood as indicators for external or surface remodeling. Note that for reasons of visualization, material surface forces on the fixed boundary that appear as a natural reaction to the constraint placed by fixing material node point positions in the reference configuration are not included in the plot of Fig. 6.

In summary, this example has convincingly demonstrated the application of the material force method to bone remodeling. The knowledge of material forces provides additional insight into the biologically induced rearrangement of material inhomogeneities inside the specimen and the reorganization of structural surfaces.

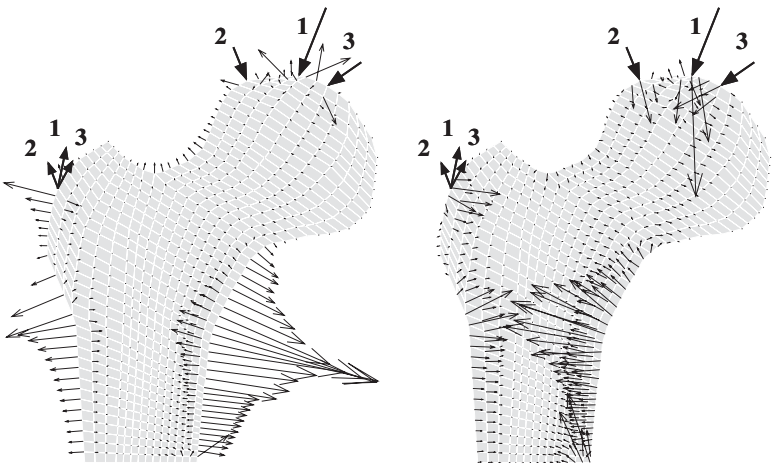

Fig. 6. Proxima femur—material surface and volume forces $F^{\Phi h}_{\text{sur}}$ and $F^{\Phi h}_{\text{vol}}$.

7.3. Biomechanics: healing

The final example is originally borrowed from non-linear elastic fracture mechanics. It represents the qualitative study of healing in a single edge notched specimen subjected to tensile loading. The specimen is of rectangular shape with a length of $l = 225$ and a width of $w = 75$ units. The corresponding finite element discretization consisting of 3565 node points and 1140 finite elements is depicted in Fig. 8 (top). Eight-noded serendipity elements are applied throughout except for the crack tip close to which we apply quadratic triangles. A close-up of the heavily defined mesh at the crack tip is given in Fig. 8, bottom. The Lamé constants are chosen similar to the previous example as $\lambda = 138.89$ and $\mu = 208.33$. Again, the two exponents are taken as $n = 2$ and $m = 3$, the reference density is chosen to $\rho_0^* = 1.00$ and the mass flux is neglected as $R_0 = 0$. Since we aim at subjecting the specimen to large strains, the value of the reference free energy has been enlarged by a factor 50 in comparison to the previous example, thus $\Psi_0^* = 0.50$. Moreover, the analysis of large strains requires a step wise application of the total load. The specimen is thus loaded by a ramp load over 10 time steps of $\Delta t = 0.05$ each, by an incrementally increasing spatial force of $\Delta \boldsymbol{f}_{\text{sur}}^{\varphi} = 250$ applied on the upper and lower boundary. The 10 load steps are depicted in Fig. 7, left. Once the final load level of $\boldsymbol{f}_{\text{sur}}^{\varphi} = 2500$ is reached, the load is held constant for another 50 time steps of $\Delta t = 0.05$ while the density distribution converges towards the biological equilibrium state.

Fig. 7 (left), shows the prescribed spatial force f_{sur}^{φ} scaled by a factor 250 and the corresponding evolution of the crack opening δ on the left boundary as a result of the spatial motion problem. As the load is increased, the crack opening δ increases correspondingly up to approximately 5% of the total specimen length. However, during the phase of constant loading from $t = 0.5$ to $t = 3.0$, a clear tendency towards self-healing can be observed. The healing process manifests itself in a considerable closing of the crack to about two third of its maximum size. Fig. 8 (top), supports this observation. It shows the deformed configurations corresponding to $t = 0.25$ right in the middle of the loading phase, $t = 0.50$ at the end of the loading phase and $t = 3.0$ close to biological equilibrium.

The total deformation increases during the loading phase but then decreases again during the phase of constant loading. The decrease in deformation and the corresponding closure of the crack illustrate the biomechanical coupling. They can be explained by the apposition of new material close to the crack tip which can be interpreted as a biomechanically induced self-healing process. The density contours depicted in Fig. 8 indicate an enormous increase in density close to the crack tip while material is resorbed locally near the stress free crack faces.

Let us now turn to the solution of the material motion problem and analyze the evolution of the material forces. Fig. 7 (right), depicts the material force F_{sur}^{Φ} at the crack tip which increases during the loading phase but then relaxes towards a remarkably lower value at biological equilibrium. Apparently, due to the

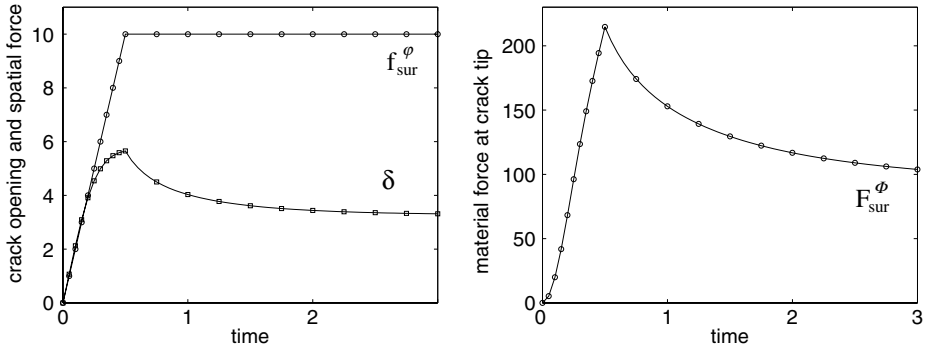

Fig. 7. Crack—evolution of crack opening δ and material forces at crack tip F_{sur}^{Φ}.

apposition of new material close to the crack tip, the absolute value of the material force could be reduced considerably up to about 60% of its maximum value. The spatial distribution of the discrete material surface forces $\boldsymbol{F}^{\Phi}_{\text{sur}}$ and the corresponding discrete volume forces $\boldsymbol{F}^{\Phi}_{\text{vol}}$ are depicted in Fig. 8. Note that for the sake of visualization, the nodal volume forces have been magnified by a factor 50 in comparison to the corresponding surface terms. Again, the discrete material volume forces are essentially orthogonal to the

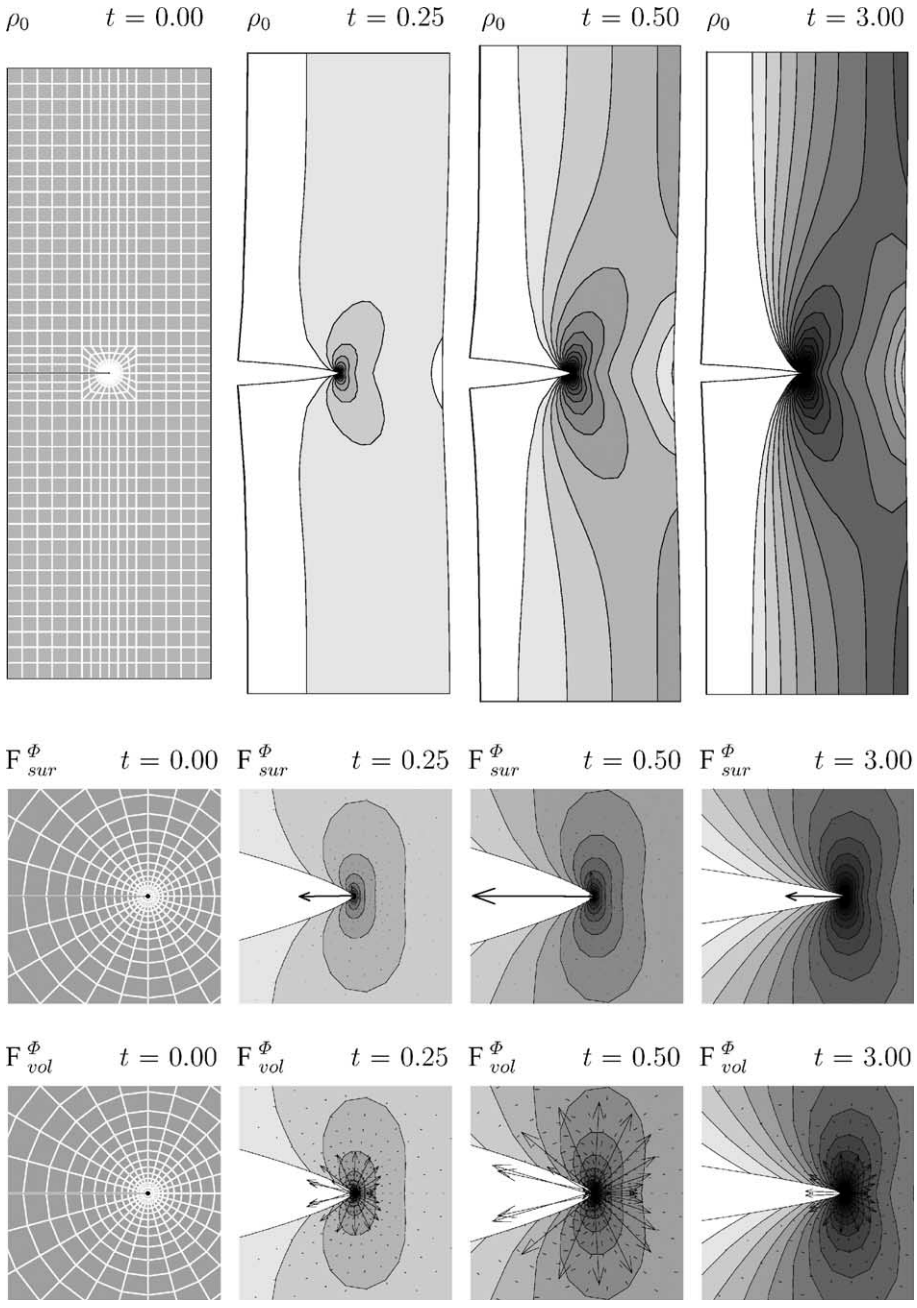

Fig. 8. Crack—evolution of density ρ_0, material surface and volume forces F^{Φ}_{sur} and F^{Φ}_{vol}.

isolines of the density contour plot. Both, the surface and volume forces increase upon loading but show a relaxation at constant applied load.

Discrete material surface forces typically point in the direction of a potential energy increase upon replacement of the material node point positions. They thus indicate, that the apposition of new material opposite to this direction would reduce the potential energy. Exactly this property is reflected by the balance of mass for open systems in combination with an appropriate constitutive assumption for the source term $\mathscr{R}_0$. For the free energy based approach considered herein, the balance of mass at biological equilibrium with $\mathrm{D}_t\rho_0 = 0$ can be rewritten as $[\rho_0^*/\rho_0]^{m-n}\Psi_0 = \Psi_0^*$. If the value of the reference free energy Ψ_0^* is locally exceeded, the apposition of new material with $\rho_0 > \rho_0^*$ essentially helps to decrease the value of the free energy based biological stimulus $[\rho_0^*/\rho_0]^{m-n}\Psi_0$, since $m > n$. As the biological stimulus approaches the attractor stimulus Ψ_0^*, the absolute value of the corresponding material surface force decreases indicating that enough material has been created to support the applied load.

Especially this last example has shown the relevance of material forces in biomechanical applications. Unlike engineering materials, biomaterials show the remarkable ability to react to changes in the environmental situation in the form of self-healing. In this context, material forces can be utilized to locate areas of potential material apposition and to improve the understanding of biomechanically induced self-healing phenomena.

8. Conclusion

The objective of the present work was the theoretical and numerical exploitation of the notion of material forces in open system mechanics. To this end, we have highlighted the fundamental duality between the classical spatial and the material point of view. Both, the spatial and the material motion set of governing equations have been reformulated in their weak form and discretized in space to set the stage for a Galerkin type finite element analysis. While the spatial motion problem typically renders the discrete node point values of the density and deformation, the material force method requires the solution of the former and can be considered as a mere post-processing step. The determination of the discrete material node point forces is thus computationally cheap and extremely straightforward once the spatial motion problem has been solved.

The computed discrete material node point forces are energetically conjugate to variations of material node point positions. Especially in the context of biomechanics, they can be computed effectively to provide on the one hand an indicator for the biomechanically induced rearrangement of material inhomogeneities responsible for internal remodeling processes. On the other hand, material forces on the specimen boundary can be interpreted as a measure of shape sensitivity indicating the tendency towards surface changes in the form of external remodeling. Pointing from high to low density concentrations, discrete material volume forces motivate the incorporation of a mass flux being essentially proportional to the density gradient. This additional mass flux tends to equilibrate concentrations and also smoothes spurious oscillations of the density field close to spatial discontinuities. Its influence is, however, typically more pronounced in soft rather than in hard tissue mechanics. Discrete material surface forces typically point into the direction of a potential energy increase upon replacement of material node point positions. Consequently, they can be applied to locate areas of potential material apposition in the opposite direction. These findings have been underlined computationally by a systematic study of selected model examples.

Although the full potential of the material force method in open system mechanics cannot be entirely foreseen at this early stage of research, the presented theoretical and algorithmic framework is believed to be extremely powerful in giving further insight into the complex mechanical processes that drive the local reorganization of inhomogeneities particularly in biomechanics. Potential biomechanical applications of functional adaption, healing, growth and morphogenesis constitute branches of ongoing research.

Appendix A

To solve the discrete coupled non-linear system of equations of the spatial motion problem, we suggest a monolithic solution strategy based on the consistent linearization of the governing equations. The discrete balance of mass $(54)_1$ and the discrete mass specific balance of momentum $(54)_2$ thus have to be solved simultaneously. To this end, we apply an incremental iterative Newton–Raphson solution procedure supplemented by the consistent linearization of the governing equations at time t_{n+1}.

$$\begin{aligned} r_{I\,n+1}^{\rho\,k+1} &= r_{I\,n+1}^{\rho\,k} + \mathrm{d}r_I^{\rho} = 0 \quad \forall I = 1, n_{\mathrm{np}} \\ \boldsymbol{r}_{J\,n+1}^{\varphi\,k+1} &= \boldsymbol{r}_{J\,n+1}^{\varphi\,k} + \mathrm{d}\boldsymbol{r}_J^{\varphi} = \boldsymbol{0} \quad \forall J = 1, n_{\mathrm{np}}. \end{aligned} \tag{A.1}$$

The iterative residuals $\mathrm{d}r_I^{\rho}$ and $\mathrm{d}\boldsymbol{r}_J^{\varphi}$

$$\begin{aligned} \mathrm{d}r_I^{\rho} &= \sum_{K=1}^{n_{\mathrm{np}}} \mathrm{K}_{\rho\rho}^{IK} \mathrm{d}\rho_K + \sum_{L=1}^{n_{\mathrm{np}}} \mathbf{K}_{\rho\varphi}^{IL} \cdot \mathrm{d}\boldsymbol{\varphi}_L \quad \forall I = 1, n_{\mathrm{np}}, \\ \mathrm{d}\boldsymbol{r}_J^{\varphi} &= \sum_{K=1}^{n_{\mathrm{np}}} \mathbf{K}_{\varphi\rho}^{JK} \mathrm{d}\rho_K + \sum_{L=1}^{n_{\mathrm{np}}} \mathbf{K}_{\varphi\varphi}^{JL} \cdot \mathrm{d}\boldsymbol{\varphi}_L \quad \forall J = 1, n_{\mathrm{np}} \end{aligned} \tag{A.2}$$

can be expressed in terms of the iteration matrices $\mathbf{K}_{\rho\rho}^{IK}$, $\mathbf{K}_{\rho\varphi}^{IL}$, $\mathbf{K}_{\varphi\rho}^{JK}$ and $\mathbf{K}_{\varphi\varphi}^{JL}$ and the incremental changes of the global vector of unknowns $\mathrm{d}\rho_K$ and $\mathrm{d}\boldsymbol{\varphi}_L$. For the problem at hand, these iteration matrices which can be interpreted as submatrices of the global tangential stiffness matrix take the following format.

$$\begin{aligned} \mathbf{K}_{\rho\rho}^{IK} &= \frac{\partial r_I^{\rho}}{\partial \rho_K} = \mathop{\mathbf{A}}_{e=1}^{n_{\mathrm{el}}} \int_{\mathscr{B}_0} N^i \frac{1}{\Delta t} N^k - N^i \partial_{\rho_0} \mathscr{R}_0 N^k + \nabla_X N^i \cdot R_0 \nabla_X N^k \, \mathrm{d}V, \\ \mathbf{K}_{\rho\varphi}^{IL} &= \frac{\partial r_I^{\rho}}{\partial \boldsymbol{\varphi}_L} = \mathop{\mathbf{A}}_{e=1}^{n_{\mathrm{el}}} \int_{\mathscr{B}_0} -N^i \partial_{\boldsymbol{F}} \mathscr{R}_0 \cdot \nabla_X N^l \, \mathrm{d}V, \\ \mathbf{K}_{\varphi\rho}^{JK} &= \frac{\partial \boldsymbol{r}_J^{\varphi}}{\partial \rho_K} = \mathop{\mathbf{A}}_{e=1}^{n_{\mathrm{el}}} \int_{\mathscr{B}_0} \nabla_X N^j \cdot \partial_{\rho_0} \overline{\boldsymbol{\Pi}}^t N^k \, \mathrm{d}V, \\ \mathbf{K}_{\varphi\varphi}^{JL} &= \frac{\partial \boldsymbol{r}_J^{\varphi}}{\partial \boldsymbol{\varphi}_L} = \mathop{\mathbf{A}}_{e=1}^{n_{\mathrm{el}}} \int_{\mathscr{B}_0} N^j \rho_0 \frac{1}{\Delta t} \boldsymbol{I} N^l + \nabla_X N^j \cdot \partial_{\boldsymbol{F}} \overline{\boldsymbol{\Pi}}^t \cdot \nabla_X N^l \, \mathrm{d}V. \end{aligned} \tag{A.3}$$

Finally, the solution of the linearized system of Eqs. (A.1) defines the iterative update for the incrementals of the global unknowns ρ_I and $\boldsymbol{\varphi}_J$.

$$\begin{aligned} \Delta\rho_I &= \Delta\rho_I + \mathrm{d}\boldsymbol{\rho}_I \quad \forall I = 1, n_{\mathrm{np}}, \\ \Delta\boldsymbol{\varphi}_J &= \Delta\boldsymbol{\varphi}_J + \mathrm{d}\boldsymbol{\varphi}_J \quad \forall J = 1, n_{\mathrm{np}}. \end{aligned} \tag{A.4}$$

Remark A.1. Recall, that when considering the reduced balance of momentum in the quasi-static sense, the term $N^J \rho_0 / \Delta t \boldsymbol{I} N^L$ of Eq. $(A.3)_4$ vanishes identically.

References

[1] H. Askes, E. Kuhl, P. Steinmann, An ALE formulation based on spatial and material settings of continuum mechanics. Part 2: Classification and applications, Comput. Methods Appl. Mech. Engrg., in press.

[2] G.S. Beaupré, T.E. Orr, D.R. Carter, An approach for time-dependent bone modelling and remodelling, J. Orth. Res. 8 (1990) 651–670.

[3] M. Braun, Configurational forces induced by finite-element discretizations, Proc. Estonian Acad. Sci. Phys. Math. 46 (1997) 24–31.

[4] D.R. Carter, G.S. Beaupré, Skeletal Function and Form—Mechanobiology of Skeletal Development, Aging and Regeneration, Cambridge University Press, 2001.
[5] D.R. Carter, W.C. Hayes, The behavior of bone as a two-phase porous structure, J. Bone Joint Surg. 59-A (1977) 785–794.
[6] S.C. Cowin, D.H. Hegedus, Bone remodelling I: Theory of adaptive elasticity, J. Elasticity 6 (1976) 313–326.
[7] R. Denzer, F.J. Barth, P. Steinmann, Studies in elastic fracture mechanics based on the material force method, Int. J. Num. Methods Engrg. 58 (2003) 1817–1835.
[8] M. Epstein, G.A. Maugin, The energy–momentum tensor and material uniformity in finite elasticity, Acta Mech. 83 (1990) 127–133.
[9] M. Epstein, G.A. Maugin, Thermomechanics of volumetric growth in uniform bodies, Int. J. Plasticity 16 (2000) 951–978.
[10] J.D. Eshelby, The force on an elastic singularity, Philos. Trans. Roy. Soc. Lond., A 244 (1951) 7–112.
[11] J.D. Eshelby, The determination of the elastic field of an ellipsoidal inclusion and related problems, Proc. Roy. Soc. Lond. A 241 (1957) 376–396.
[12] L. Gambarotta, R. Massabo, R. Morbiducci, E. Raposio, P. Santi, In vivo experimental testing and model identification of human scalp skin, J. Biomech., in press.
[13] K. Garikipati, H. Narayanan, E.M. Arruda, K. Grosh, S. Calve, Material forces in the context of bio-tissue remodelling, in: P. Steinmann, G.A. Maugin (Eds.), Proc. Euromech Colloquium 445 'Mech. Mater. Forces', Kluwer Academic Publishers, 2003.
[14] L.J. Gibson, M.F. Ashby, The mechanics of three-dimensional cellular materials, Proc. Roy. Soc. Lond. A 382 (1982) 43–59.
[15] S. Govindjee, Firestone Tire Analysis, Internal Report, Lafayette, CA, 2001.
[16] M.E. Gurtin, On the nature of configurational forces, Arch. Rat. Mech. Anal. 131 (1995) 67–100.
[17] M.E. Gurtin, Configurational Forces as Basic Concepts of Continuum Physics, Springer Verlag, New York–Berlin–Heidelberg, 2000.
[18] T.P. Harrigan, J.J. Hamilton, Optimality condition for finite element simulation of adaptive bone remodeling, Int. J. Solids Struct. 29 (1992) 2897–2906.
[19] T.P. Harrigan, J.J. Hamilton, Finite element simulation of adaptive bone remodelling: A stability criterion and a time stepping method, Int. J. Num. Methods Engrg. 36 (1993) 837–854.
[20] J.D. Humphrey, Cardiovasular Solid Mechanics, Springer Verlag, Berlin–Heidelberg–New York, 2002.
[21] C.R. Jacobs, M.E. Levenston, G.S. Beaupré, J.C. Simo, D.R. Carter, Numerical instabilities in bone remodeling simulations: The advantages of a node-based finite element approach, J. Biomech. 28 (1995) 449–459.
[22] C.R. Jacobs, J.C. Simo, G.S. Beaupré, D.R. Carter, Adaptive bone remodeling incorporating simultaneous density and anisotropy considerations, J. Biomech. 30 (1997) 603–613.
[23] R. Kienzler, G. Herrmann, Mechanics in Material Space with Applications in Defect and Fracture Mechanics, Springer Verlag, Berlin–Heidelberg–New York, 2000.
[24] E. Kuhl, P. Steinmann, Mass and volume specific views on thermodynamics for open systems, Proc. Roy. Soc. Lond. 459 (2003) 2547–2568.
[25] E. Kuhl, P. Steinmann, On spatial and material settings of thermo-hyperelastodynamics for open systems, Acta Mech. 160 (2003) 179–217.
[26] E. Kuhl, P. Steinmann, Theory and numerics of geometrically non-linear open system mechancis, Int. J. Num. Methods Engrg. 58 (2003) 1593–1615.
[27] E. Kuhl, A. Menzel, P. Steinmann, Computational modeling of growth: A critical review, a classification of concepts and two new consistent approaches, Comput. Mech. 32 (2003) 71–88.
[28] E. Kuhl, P. Steinmann, Computational modeling of healing: An application of the material force method, Biomech. Mod. Mechanobiol., in press.
[29] E. Kuhl, R. Denzer, F.J. Barth, P. Steinmann, Application of the material force method to thermo-hyperelasticity, Comput. Meth. Appl. Mech. Engrg., in press. PII: S0045-7825(04)00136-7. doi:10.1016/j.cma.2003.09.021.
[30] E. Kuhl, H. Askes, P. Steinmann, An ALE formulation based on spatial and material settings of continuum mechanics. Part 1: Generic hyperelastic formulation, Comput. Methods Appl. Mech. Engrg., in press.
[31] T. Liebe, R. Denzer, P. Steinmann, Application of the material force method to isotropic continuum damage, Comput. Mech. 30 (2003) 171–184.
[32] G.A. Maugin, Material Inhomogenities in Elasticity, Chapman & Hall, London, 1993.
[33] G.A. Maugin, Material forces: Concepts and applications, Appl. Mech. Rev. 48 (1995) 213–245.
[34] R. Müller, S. Kolling, D. Gross, On configurational forces in the context of the finite element method, Int. J. Num. Methods Engrg. 53 (2002) 1557–1574.
[35] R. Müller, G.A. Maugin, On material forces and finite element discretizations, Comput. Mech. 29 (2002) 52–61.
[36] H.E. Pettermann, T.J. Reiter, F.G. Rammerstorfer, Computational simulation of internal bone remodeling, Arch. Comput. Meth. Engrg. 4 (1997) 295–323.
[37] T.J. Reiter, Functional Adaption of Bone and Application in Optimal Structual Design, VDI Berichte Reihe 17, Nr. 145, VDI-Verlag, Düsseldorf, 1996.

[38] E.K. Rodriguez, A. Hoger, A.D. Mc Culloch, Stress-dependent finite growth in soft elastic tissues, J. Biomech. 27 (1994) 455–467.
[39] R.T. Shield, Inverse deformation results in finite elasticity, ZAMP 18 (1967) 490–500.
[40] M. Silhavý, The Mechanics and Thermodynamics of Continuous Media, Springer Verlag, New York–Berlin–Heidelberg, 1997.
[41] P. Steinmann, On spatial and material settings of hyperelastodynamics, Acta Mech. 156 (2002) 193–218.
[42] P. Steinmann, On spatial and material settings of thermo-hyperelastodynamics, J. Elasticity 66 (2002) 109–157.
[43] P. Steinmann, D. Ackermann, F.J. Barth, Application of material forces to hyperelastostatic fracture mechanics. II. Computational setting, Int. J. Solids Struct. 38 (2001) 5509–5526.
[44] L.A. Taber, Biomechanics of growth, remodeling, and morphogenesis, ASME Appl. Mech. Rev. 48 (1995) 487–545.
[45] H. Weinans, R. Huiskes, H.J. Grootenboer, The behavior of adaptive bone-remodeling simulation models, J. Biomech. 25 (1992) 1425–1441.
[46] H. Weinans, R. Huiskes, H.J. Grootenboer, Effects of fit and bonding characteristics of femoral stems on adaptive bone remodeling, J. Biomech. Eng. 116 (1994) 393–400.
[47] J. Wolff, Das Gesetz der Knochentransformation, Hirschwald, Berlin, 1892.